Towards Longitudinal Control for Over-the-Horizon Autonomous Convoying

by

Anjani Kulani

A thesis submitted in conformity with the requirements
for the degree of Master of Applied Science
Graduate Department of Electrical and Computer Engineering
University of Toronto

Abstract

Towards Longitudinal Control for Over-the-Horizon Autonomous Convoying

Anjani Kulani

Master of Applied Science

Graduate Department of Electrical and Computer Engineering

University of Toronto

2013

In a variety of military operations, there is a need for a convoy of autonomous followers to traverse the leader's path without using Global Positioning System (GPS), lane markers/magnets and/or a vision-based vehicle-following system. This can be achieved by using Visual Teach and Repeat (VT&R), which provides an effective method for autonomous repeating of a previously driven path. This thesis describes the design of a distributed control system that uses the idea behind the VT&R method to allow a convoy of inter-communicable autonomous vehicles to follow a manually-driven lead vehicle's path with a desired inter-vehicle spacing, even when the leader is not in the camera view of the followers. The longitudinal controller is designed for addressing a 1D spacing problem and then combined with a path tracker for tracking a path in a 2D environment. The designed control model is tested in simulations, which show satisfactory performance over a range of operating conditions.

Acknowledgements

I would like to thank my co-supervisors, Professor Bruce Francis and Professor Tim Barfoot, for all the time they have invested in guiding me through my studies. I am greatly indebted to Professor Francis for his immense patience and keen attention to all the writing details which has helped me to improve my writing style, and to Professor Barfoot for all the practical guidance throughout the thesis.

I also want to thank Keith Leung for sharing his technical expertise and Siddhartha Kumar for his support when the going was tough.

This work would not have possible without the support and love of my parents. I thank them for their encouragement and the sacrifices they have made for helping me achieve my goals.

Contents

List of Tables

List of Figures

Chapter 1

Introduction

1.1 Motivation

Increasing autonomy in military operations has been an ongoing task for decades. Scenarios where a manned vehicle convoy traverses a hostile environment may lead to high operation costs and possibly to loss of human lives. So, a convoy of autonomous follower vehicles can be used, whereby each follower vehicle can use the GPS, lane markers/magnets, and/or a vision-based vehicle-following system to follow the leader's path. However, in a hostile territory reliable GPS signals may not be available and the roads may be unpaved with no provisions for setting magnets/markers. A vision-based vehicle-following system has already been studied by Goi et al. (2010). A review of the work done by Goi (2009) is presented in the next section.

1.2 Review of Goi's Thesis

In this project, the goal was to use only onboard sensors to enable a convoy of autonomous follower vehicles to track the trajectory of a manually-driven leader. The use of GPS, lane markers/ magnets, and/or inter-vehicle communication was prohibited. The convoy was decomposed into identical leader-follower pairs and the goal of an autonomous follower was to track the trajectory of its immediate leader delayed by a constant time, τ, as shown in Figure 1.1. Here, $\big(x(t), y(t)\big)$ is the follower's position with respect to an inertial frame and $\big(x_0(t), y_0(t)\big)$ is the leader's position with respect to the same frame. The follower aims to track the delayed leader's position defined as $\big(x_d(t), y_d(t)\big) := \big(x_0(t-\tau), y_0(t-\tau)\big)$. Thus, the following distance depends on the leader's speed and "future" delayed-leader

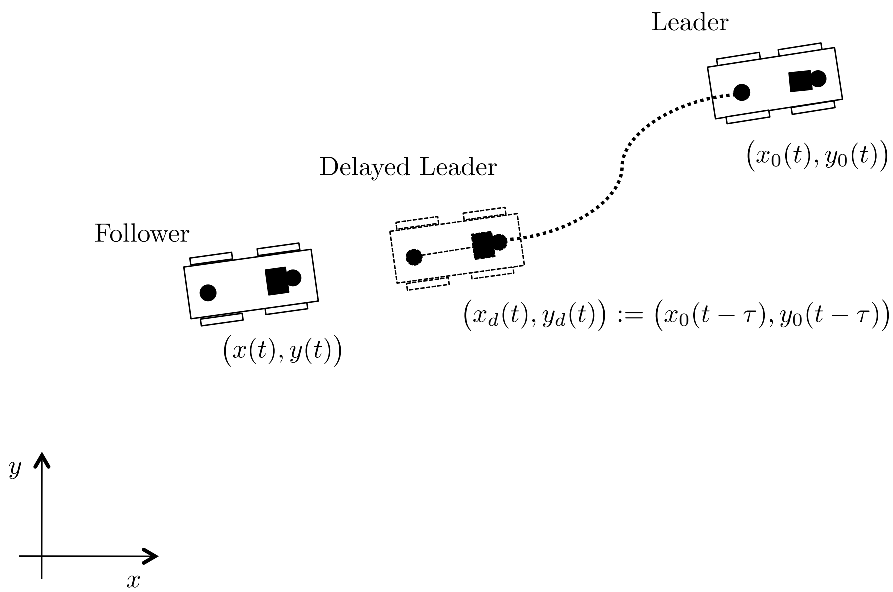

Figure 1.1: Defining the delayed leader $\big($courtsey Goi (2009)$\big)$.

positions are available because of the measurements up to the leader's current position.

As the experiments were performed on the MultiAgent Tactical Sentry (MATS) vehicle, the onboard sensors available were a monocular camera and wheel encoders. The block diagram of the vehicle-following system for an autonomous follower is shown in Figure 1.2, where the positions and heading are relative to an inertial frame. The output of the follower's camera is the measured range, ρ_m, and measured bearing, ϕ_m, to its leader. The wheel encoders output the measured speed, v_m, and measured steering, γ_m, of the follower. The vehicle-following system uses these signals to produce the follower's commanded speed, v_c, and commanded steering, γ_c. The actual speed and steering of the follower is represented by v and γ, respectively and the follower's actual heading is

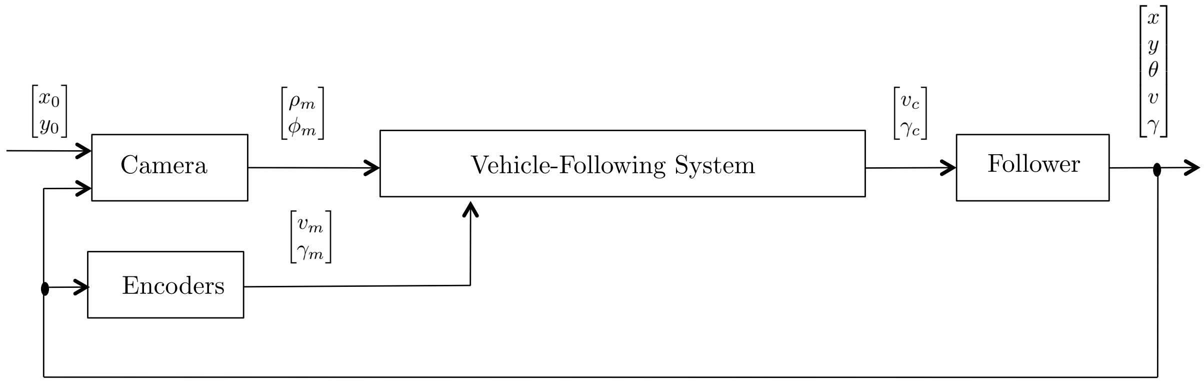

Figure 1.2: Block diagram of the vehicle-following system for an autonomous follower (courtsey Goi (2009)).

denoted by θ.

The follower kinematics is presented by the bicycle model as shown in Figure 1.3. The state of the model are the back wheel's position, (x, y), and its heading, θ and the inputs are the rear wheel's translational speed, v, and the front wheel's turning angle, γ. The distance between the front and rear wheels is represented by d.

A two-tier architecture was used to represent the vehicle model, where the speed-and-steering control system regulates the vehicle dynamics while the kinematics is regulated by the vehicle-following system as shown in Figure 1.4a. The reference signal to the inner loop is the commanded speed and steering angle, (v_c, γ_c), and the output signal is the actual speed and steering angle, (v, γ). The inner-loop can be treated as a unity gain if the bandwidth separation between the two loops is sufficient as shown by Kokotovic et al. (1999), that is, the inner-loop's operating frequency is high enough so that the dynamics of the vehicle can be neglected and only the kinematic model is used to represent the follower's model as shown in Figure 1.4b. Under this assumption, $v = v_c$ and $\gamma = \gamma_c$. Therefore, the equations for the follower's kinematics model are

$$\dot{x} = v_c \cos\theta$$

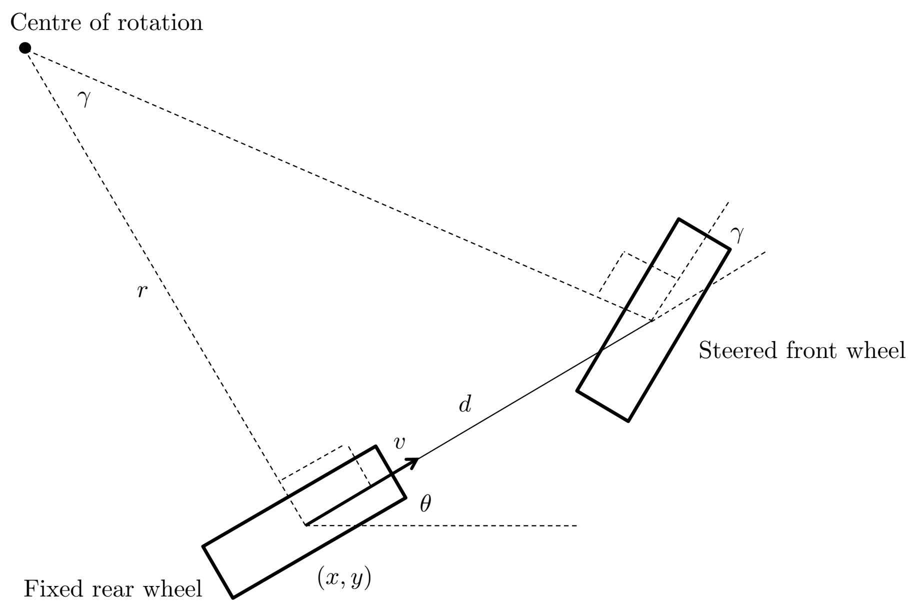

Figure 1.3: Bicycle model (courtsey Goi (2009)).

$$\dot{y} = v_c \sin\theta$$
$$\dot{\theta} = \frac{v_c}{d}\tan\gamma_c.$$

The longitudinal and lateral errors are defined as

$$\begin{bmatrix}\varepsilon_1 \\ \varepsilon_2\end{bmatrix} := \begin{bmatrix}\cos\theta_d & \sin\theta_d \\ -\sin\theta_d & \cos\theta_d\end{bmatrix}\begin{bmatrix}x_d - x \\ y_d - y\end{bmatrix},$$

where (x_d, y_d) is the position and θ_d is the heading of the delayed leader, and the heading error is given as

$$\varepsilon_3 = \theta_d - \theta.$$

The vehicle model obtained by linearizing about a constant-velocity trajectory is

$$\dot{\varepsilon}_1 = v_d - v_c$$
$$\dot{\varepsilon}_2 = v_d\varepsilon_3$$
$$\dot{\varepsilon}_3 = -\frac{v_d}{d}\gamma_c,$$

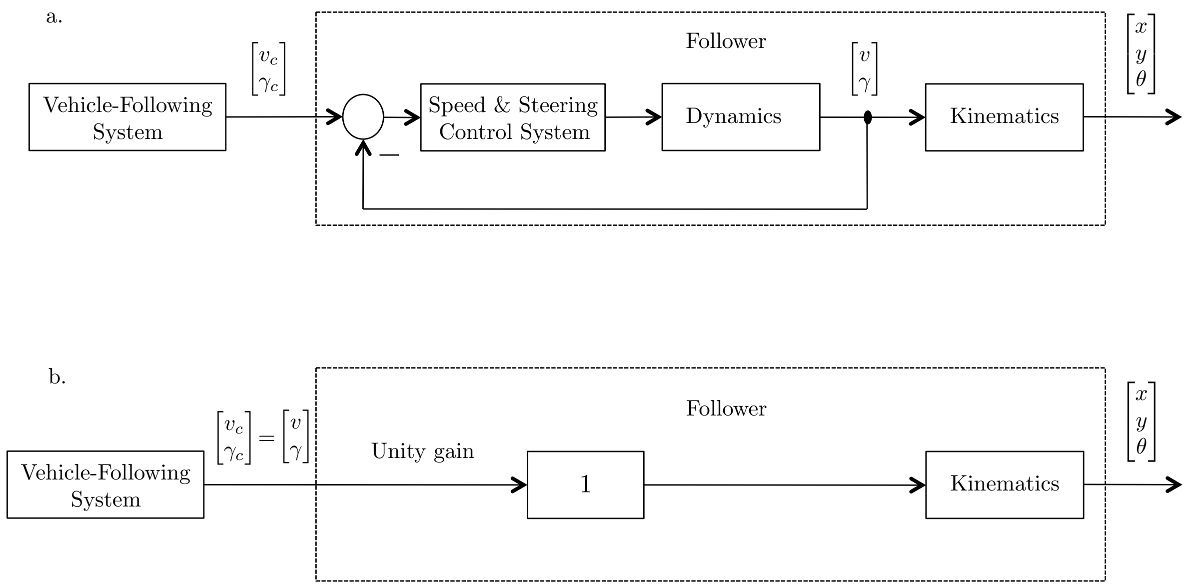

Figure 1.4: Figure 1.2 shows (v, γ) also as output, but this is omitted here. (a) Inner/outer loop architecture for the follower . (b) The outer-loop controller is designed by assuming that the inner loop is a unity gain.

where v_d is the speed of the delayed leader. After some initial experiments, the model was modified to account for road slope and large longitudinal error on straightaways caused by slow throttle dynamics, which has been modeled by the unity gain inner loop. Thus, the linearized model used in the experiments was

$$\begin{aligned}
\dot{\varepsilon}_1 &= v_d - v_c + \delta_1 \\
\dot{\varepsilon}_2 &= v_d \varepsilon_3 \\
\dot{\varepsilon}_3 &= -\frac{v_d}{d}(\gamma_c + \delta_2).
\end{aligned}$$

Here δ_1 represents the model uncertainty and δ_2 is the constant bias that accounts for the slope.

As the above model is decoupled in the lateral and longitudinal directions, the longitudinal control is given as

$$v_c = v_d + k_{p,1}\varepsilon_1 + k_{i,1} \int_0^t \varepsilon_1(q)dq$$

and the lateral control is given by

$$\gamma_c = k_{p,2}\varepsilon_2 + k_{i,2}\int_0^t \varepsilon_2(q)dq + k_{p,3}\varepsilon_3,$$

where the $k's$ are the controller gains. A constant-time look-ahead feature was added to compensate for large lateral error occurring at turns. Thus, the heading error is computed by

$$\varepsilon_3 = \theta_l - \theta,$$

where θ_l is the heading of the look-ahead point.

A heading gyro was later added to the MATS vehicle to measure the vehicle's heading, θ_m. As the controller requires the signals (x, y, θ), (x_d, y_d, θ_d), and θ_l which cannot be measured directly, other than θ, a nonlinear observer was used to estimate the unmeasurable signals. The nonlinear observer used dead reckoning to estimate the follower's position, $(\hat{x}, \hat{y})$. For smoothing the camera measurements, a summation of cubic splines was used to fit a curve to the measurements. Thus, an estimate, $(\hat{x}_d, \hat{y}_d)$, of the delayed leader's position was obtained. A line-fitting window was used to estimate the delayed leader's speed, $\hat{v}_d$, and heading, $\hat{\theta}_d$, along with the look-ahead position's heading, $\hat{\theta}_l$. The top-level block diagram of the system with the heading gyro is shown in Figure 1.5.

Limitations

Though successful experiments were carried out with one and two followers, nevertheless, the model is not robust to increasing follower number, high operating speeds, and lighting changes. This vision-based system will also fail if the leader goes out of line of sight of the follower for a considerable duration of time, e.g., when negotiating a turn around a building's corner.

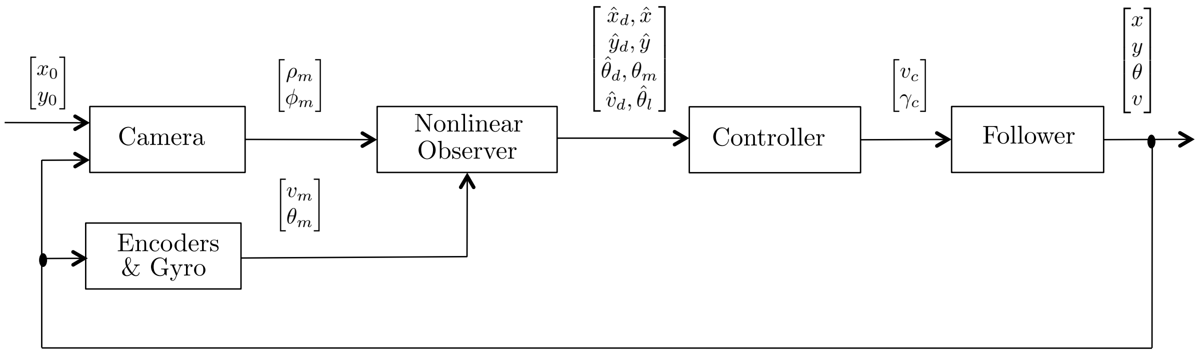

Figure 1.5: Top-level block diagram of the overall system with the heading gyro added to the model (courtsey Goi (2009)).

1.3 Other Related Work

For making a vehicle traverse a path, the concept of Visual Teach and Repeat (VT&R) can be incorporated, which provides an effective method for autonomous repeating of a previously driven trajectory without using GPS. Successful experiments on the implementation of VT&R were done by Furgale and Barfoot (2010) and McManus et al. (2012). There are two parts to the VT&R method, as discussed in the work by Furgale and Barfoot (2010): the teach pass and the repeat pass. The route teaching, called the teach pass, is comprised of driving a vehicle on a desired route while a visual sensor captures images. These images are logged and are then post-processed into a series of locally consistent overlapping maps, with 3D landmarks embedded within each local map. During the repeat pass, the archived submaps are used for localization, that is, the vehicle references the stored submaps and compares current views with the previously seen views so as to autonomously traverse the taught trajectory.

The method described by Furgale and Barfoot (2010) has been further improvised by McManus et al. (2012) so that the map building occurs online and instead of locally consistent submaps, augmented keyframes are used to represent local maps, amongst other improvements.

However, in the works of both Furgale and Barfoot (2010) and McManus et al. (2012), the teach and repeat pass is executed on the same vehicle.

Hedrick et al. (1991) showed that for a platoon of vehicles, the inter-vehicle spacing error got amplified with increasing follower number. Working in this area, Swaroop and Hedrick (1996) introduced the notion of string stability and derived sufficient conditions to ensure the boundedness of the state of an interconnected system. For a vehicle-following system, they proved that the longitudinal spacing error did not grow on adding more follower vehicles. Swaroop et al. (2001) showed string stability for a platoon of vehicles even in the presence of parametric uncertainty. They developed a decentralized adaptive control algorithm that guaranteed zero steady-state spacing errors and uniform boundedness of spacing errors under some mild assumptions. Simulation results are shown for a five vehicle platoon to validate the controller design. The spacing error goes to zero and the maximum spacing error is about 0.12 m with the adaptive control.

1.4 Objectives of the Thesis

This thesis is an extension of the work done by Goi et al. (2010) and aims to address the limitations detailed in Section 1.2. It aims to remove the upper-bound on the length of convoy so that increasing follower number still leads to robust performance. Another salient feature is to enable leader's path tracking even when the leader is not in the camera view of the follower. It also attempts to extend the VT&R method to a convoy problem. The VT&R method by itself ensures that each of the followers tracks the leader's path but it does not handle the inter-vehicle spacing problem. This thesis attempts to use the VT&R method to control the inter-vehicle distance. It should be noted that the effect of lighting changes can only be addressed when the laser-based VT&R method is used for convoying as discussed by McManus et al. (2012).

For this thesis, the problem setup consists of a convoy of autonomous follower vehicles and a manually-driven leader moving in a terrain. The vehicles are equipped with wheel encoders and a monocular camera, and have computational capability. In Goi et al. (2010), the vehicles are not allowed to communicate with each other and each vehicle can see the one in front. Here, we relax these constraints and allow the vehicles to communicate with each other and assume that the leader is not in the camera view of all the followers. For incorporating the concept of VT&R, we further postulate that there are landmarks that can be used for building maps. For the above described convoy problem, the teach pass and the repeat pass occur simultaneously, that is, the leader constructs a map as it travels and communicates the map to all the followers via radio communication. The map communicated by the leader is stored by all the followers. Each of the followers repeats the leader's path by referencing the leader's archived map and comparing its current view with the previously seen views by the leader. Thus, the leader and all the followers travel together and the leader performs the teach pass while all the followers execute the repeat pass simultaneously.

With the above background, the goal is to investigate the viability of the concept that uses the idea behind the VT&R method to allow a convoy of inter-communicable autonomous vehicles to follow a manually-driven lead vehicle's path with a desired inter-vehicle spacing, even when the leader is not in the camera view of the followers.

1.5 Overview of Distributed Mobile Robotics

The field of mobile distributed robots started gaining importance in the late 1980's. Some of the topics of interest during this time were reconfigurable robot systems, such as the work on the Cellular Robotic System (CEBOT) by Fukuda and Nakagawa (1987), multi-robot planning, like the work on traffic control by Premvuti and Yukta (1990), and the work on ACTRESS by Asama et al. (1989) for developing an architecture for multi-robot cooperation. Since then, significant progress has been made on a much wider variety of topics.

The introduction of behavior-based control led to the examination of biological societies like the formation of birds in a flock by Vicsek et al. (1995). Based on biological inspirations, multi-robot systems have been developed for following trails, dispersing, and flocking as shown by Deneubourg et al. (1990) and Mataric (1994). The effect of acting on selfish interests in multi-robot systems was studied as emergent cooperation by McFarland (1994).

The benefits of communication of information as presented by Balch and Arkin (1994) led to the setting up of distributed communication networks as shown by Winfield (2000). Molnar and Starke (2000) worked on ensuring reliability in multi-robot communications. Synchronized motion of a group of autonomous mobile robots was achieved by using radio communication as discussed by Ozaki et al. (1993). For scenarios with no communication infrastructure, the mobile robots could use group communication by forming an ad hoc network as demonstrated by Das et al. (2005). For improving communication efficiency, Yoshida et al. (1994) worked on the problem of the optimal group size to transmit information.

Another domain of interest has been the coordinated control of a network of autonomous mobile robots. The problem of achieving a specified formation among a group of mobile autonomous agents by distributed control is studied by Lin et al. (2003). Ando et al. (1999) developed distributed algorithm for getting autonomous mobile robots to converge towards a single point while Sinha and Ghose (2006) showed that the point of convergence in cyclic pursuit can be controlled. Marshall et al. (2004) demonstrated that in the cyclic pursuit framework, the equilibrium formations for a system of linear agents are generalized regular polygons.

Approaches to localization, mapping, and exploration can be categorized based on the use of graphs, Global Positioning System (GPS), and/or landmarks, and on the use of range sensors such as sonar or laser and vision sensors. A detailed literature review of this area is presented in the next section.

1.6 Literature Review

An important aspect in the navigation of a convoy of autonomous follower vehicles is the way the followers localize themselves in an unknown environment. A variety of approaches have been presented for the localization of the follower's current position using graphs, GPS, and/or landmarks, and on the use of range sensors such as sonar or laser and vision sensors.

Localization using vision sensors

Kehtarnavaz et al. (1991) developed a vehicle-following system that used a stereo camera mounted on their autonomous vehicle, Binocular Autonomous Research Team (BART), to track the leader and obtain the range and bearing. The experimental trials were performed on a 1.5 km test track and the desired following distance was set to 15 m. Using only heuristic control laws, small lateral deviations are observed for speeds up to 8.9 m/s. But the experimental data is limited to two 5-minutes trials and the range to the leader varies greatly from 7 m to 60 m.

Benhimane et al. (2005) presented experimental results with two electric vehicles called "Cycab" on a 100 m closed loop with the goal of tracking a virtual leader rigidly linked at a constant distance behind the leader. A pan-tilt camera was used to keep the leader in the field of view of the follower during tight turns. However, since the path of the leader was not stored, the follower may cut corners on turns. The speed of the vehicles were saturated at 1 m/s. But it is stated that on increasing the speed the intrinsic noise is very high. It is explicitly stated that the model is sensitive to lighting conditions. Results for the lateral and longitudinal errors are not included. Daviet and Parent (1996) also performed experiments with electric vehicles, but the speed of the vehicles were up to 10 m/s. Though the data is shown for only 30 s, the reported longitudinal and lateral tracking errors are under 0.3 m and 0.6 m, respectively.

In order to cope with different lighting conditions and partial occlusion of the lead vehicle, Manz et al. (2011) developed a real-time modular system to track vehicles using monocular vision. A full 3D model of the lead vehicle was developed to describe the vehicle geometry and appearance, which was used within a particle filter to estimate the 6 DoF position relative to the follower vehicle. Experimental runs were performed in a variety of outdoor environments for a 12 minutes drive with operating speeds up to 50 km/h in both forward and backward directions. The estimation of the radial distance to the lead vehicle's center of gravity has a root mean square value of approximately 0.5 m.

Klančar et al. (2011) proposed a local control strategy for vehicle platooning. The leader followed a reference trajectory which was a parametric polynomial and the follower vehicle followed the travelled path of the leader considering a required safety distance. The leader position was determined by an indoor camera on the ceiling. However, the follower used a stereo camera to determine its distance and relative orientation with respect to the leader, and odometry to calculate its position. The reference position and the orientation of the follower was determined by the estimated path of the leader. Experimental plot of the trajectories followed by the two vehicles is presented. The error values are not discussed though the trajectory self intersects itself at one point. Simulation results on increasing the follower number show that the tracking error increases with the follower number. Thus, there is a limit to the maximum number of followers that can be added.

Schneiderman et al. (1995) used radio communications to send video images from the Charged-Coupled Device (CCD) camera mounted on the follower vehicle to the follower's computer system. They demonstrated a path-following system with a 33 km traverse at speeds of 13.9 to 20.8 m/s and at following distances of 5 to 15 m. However, only the steering was autonomous and the braking and throttling was done manually. Also, the follower did not store the leader's path and visually tracked a target mounted on the back of the leader. The model was tested in a variety of lighting conditions and in presence of other vehicles. However, the model failed if the following distance was increased to greater than 20 m. Similarly, Fritz (1999) employed an image processing system to obtain relative information about the leader's and follower's positions. They used inter-vehicle communications to obtain the leader's speed and acceleration. Experiments were performed on commercial trucks as the testbed. Longitudinal tracking results are shown for a duration less than 200 s with speeds up to 20 m/s. The longitudinal tracking error is reported to be less than 2 m. For lateral tracking, test results are shown for a circular test track with a 80 m radius and the lateral error is less than 0.3 m. However, they emphasis that based on simulation results, addition of more trucks is not suited.

As the above vehicle-following systems did not store the leader's trajectory, the lateral error may grow if the following distance gets very large. Also, the systems will fail if the roads have sharp turns. Gehrig and Stein (1998) advocated the approach of following the leader's path instead of the leader itself. A solely vision-based algorithm called control using trajectory (CUT) was used to track the leader's trajectory point which was a constant distance ahead of the follower's position. Experimental results are shown for a circular path with and without CUT at speeds of 10 m/s and a following distance of 25 m for a duration of 15 s. The maximum lateral errors reported for the two experiments are 0.7 m and 1.4 m, respectively. Similarly, Goi et al. (2010) worked on the concept of making the follower track the leader's trajectory delayed by a constant time. Successful experimental trials were conducted on a 1.3 km test track with one and two followers with speeds of about 2.8 m/s. With one follower, the follower averaged a lateral error of 0.12 ± 0.28 m (mean$\pm$standard deviation) and a maximum absolute lateral error of 1.32 m over a 10-lap traverse of the test track. The absolute longitudinal error does not go to zero due to underestimation of the range measurements as the following distance increases, and the absolute lateral error also increases with path curvature as the system is based on a constant velocity controller. Therefore, a large path curvature will move the tracking farther away from its ideal conditions. In the trials with two followers, followers 1 and 2 averaged lateral errors are 0.02 ± 0.23 and 0.24 ± 0.41 m, respectively, over a 13.5-lap traverse. Follower 2's maximum lateral error after start-up is about 2 m. It is evident that the lateral error of follower 2 is amplified by the lateral error of follower 1. Simulation results with a speed of 25 m/s on straightaways and 8 m/s on a 90-degree turn show that the follower 1 and follower 2 maximum lateral errors are 3.21 ± 0.33 m and 5.15 ± 0.32 m for the 90-degree turn trajectory and 3.03 ± 0.53 m and 3.78 ± 0.55 m for the straightaway. On the other hand, Sukthankar (1993) developed a vision-based system that tracked car taillights at night. The leader's trajectory was stored as points in an intermediate map and the follower was steered from point to point. A look ahead distance of 15 m was taken for a speed of 8.9 m/s. However, the model was limited by the field of view of the camera as the model failed during sharp turns and a small following distance.

Another approach for localization using visual sensors is visual odometry, where the vehicle's motion is estimated by analyzing and tracking features obtained in the images of the surrounding environment. This obviates the need of the leader to be in camera view of the follower. This method was used by Avanzini et al. (2010) to drive three electric cars on a 115 m long trajectory with the help of inter-vehicle communication. The leader was first driven manually along the desired trajectory while a monocular camera recorded a video sequence. A 3D reconstruction of the environment was done offline. However, image distortions were seen in the 3D reconstruction of the trajectory. Therefore, a nonlinear observer based on odometry data was designed to calibrate image distortions. Thereafter, this 3D map was communicated to all the vehicles for real time localization. The speed of the leader was set to 1 m/s. The longitudinal errors of the first and second followers are shown to be within 0.14 m and 0.17 m, respectively while the lateral error results are not discussed. In a later work done by Avanzini et al. (2012) with two electric cars, the leader was driven manually but its trajectory was not prespecified. Thus, the leader's trajectory could be extended online. However, a 3D map of the environment where the vehicles planned to travel was build beforehand on similar lines as described in Avanzini et al. (2010) and supplied to each vehicle. The vehicles were driven on a 170 m closed trajectory with the leader's speed set to 1 m/s. The lateral and longitudinal errors for the follower are shown for the case when it avoids a static vehicle and they remain within 0.17 m and ±0.1 m, respectively.

Márquez-Gámez and Devy (2011) presented the approach of using a stereo cameras mounted on the leader to build a 3D map of the environment and define a path on which other followers must stay on. The 3D map consisted of a series of submaps. This is called the learning step. This map was then transmitted to followers in the replay step so that they could track the leader's path but using a different stereo camera. Only perception is considered; methods used to control the leader and the follower are not described. Experiments were only performed for the case when the leader's trajectory was repeated again on a different day by another vehicle. Only the plots of trajectories during the learning and replay mode are presented with no other information. The convoy problem has been addressed by proposing that the submaps are successively transmitted by the leader to the follower and the follower tracks the path attached to each submap.

Localization using range sensors

Using visual odometry and laser scanner, Avanzini et al. (2008) presented experiments with two electric vehicles on a 250 m U-shaped path. With a desired following distance of 6 m and the leader's speed set at 1 m/s, the longitudinal error is shown to be less than 0.1 m. On the other hand, Vasseur et al. (2004), Papadimitriou et al. (2003), and Lu and Tomizuka (2003) used only a laser scanner to measure the range and bearing to the leader. Based on these measurements, Vasseur et al. (2004) showed experiments where the follower tracked the leader on a 2 km traverse of flat roads at a speed of 8.3

m/s and a following distance of about 21 m. The maximum lateral error is shown to be 0.73 m. Papadimitriou et al. (2003) conducted low-speed experiments and the lateral error is shown to be under 0.13 m. Using the same test vehicle as Papadimitriou et al. (2003), and keeping the follower's speed and inter-vehicle distance to be 8.9 m/s and 10 m, respectively, Lu and Tomizuka (2003) reported a maximum lateral deviation of about 1 m.

A radar system was used by Haskara et al. (1997) to measure the relative velocity and the inter-vehicle distance between the lead vehicle and the follower, which are modeled as truck-trailers . Simulations were performed for the leader's speed upto 15 m/s and a following distance of approximately 12 m. The follower started with an initial following distance of 25 m and an initial speed of 12 m/s. The desired interspacing is achieved at about 60 s. Result for the lateral error is not included.

Ng and Trivedi (1996) used a sonar sensor to detect inter-vehicle distance and calculated the relative speed from two immediate distance measurements. With the help of neuro-fuzzy control, the follower tracked the leader in both forward and backward directions. The maximum speed of the leader was set to 0.1 m/s. The error plots are not shown but the speeds graph of the leader and follower suggest that the model worked well.

As a part of the Program on Advanced Technology for the Highway (PATH), Hedrick et al. (1991) proposed a control algorithm that combined the throttle/brake properties of the vehicles for controlling the inter-vehicle distance in an automated platoon of vehicles. A switching logic between the throttle and brake pressure control is also presented. However, the control algorithm requires information about the vehicle's positions. Simulation results are shown for two and four car platoon for a duration of 15 s. For two cars, the maximum longitudinal error is 0.04 m. In the simulation with four cars, the maximum spacing error is about 0.08 m and this error is shown to be increasing with follower number. In order to attenuate the problem of error accumulation, the leader's velocity and acceleration was communicated back to all the followers leading to a maximum longitudinal error of 0.04 m. Working on the PATH program, Chang et al. (1991) showed experimental results carried on Ford vehicles. A radar system was used to measure the inter-vehicle distance and a radio link was used for inter-vehicle communication. Experimental were performed for a two car platoon, where the lead vehicle was driven manually while in the follower vehicle, only the longitudinal control was automated and the test driver was responsible for lateral tracking. At a constant leader' speed of 10 m/s, the maximum spacing error is shown to be 0.6 m during the transitional control and 0.2 m during steady state. When the lead vehicle was allowed to accelerate and decelerate at a speed of 25 m/s, the maximum longitudinal error was 0.8 m for the acceleration period and stayed within 0.5 m for the rest of the time duration. With further improvements in the throttle angle control motor, the spacing error is shown to be within 0.5 m even during the acceleration time period. The theory for the above experimental trials is presented by McMahon et al. (1992).

Localization using GPS

There are a variety of GPS devices available and their accuracy may be in meters as shown by Wing et al. (2005) and Wu et al. (2002). Wu et al. (2002) studied the effectiveness of GPS and DGPS for convoy driving. Experiments were conducted on a high speed convoy of two vehicles driving at 16.7 m/s - 27.8 m/s on a 6 km long track. At the speed of 16.7 m/s, the difference in the range measurements of GPS and DGPS is as high as 20 m. However, Travis and Bevly (2008) used GPS carrier signals to estimate the relative position between two vehicles with centimeter accuracy using Dynamic base Real Time Kinematic (DRTK) algorithm and a change in position to millimeter accuracy using Time Differenced Carrier Phase (TDCP) algorithm. With the help of GPS, the follower could track the leader's path even when they were not in sight of each other. Simulation results show a maximum lateral error of 1.6 m when the following distance is

50 m.

In the works shown by Bom et al. (2005a) and Bom et al. (2005b), experiments were performed on electric vehicles equipped with laser scanners and Real-Time Kinematic (RTK) GPS and inter-vehicle communications were allowed to transmit the leader's position. In the work by Bom et al. (2005a), the desired following distance was set to 8 m and vehicle speeds were around 1 m/s. The longitudinal error is shown to be 0.007 ± 0.047 m during a 130 s test. In the experiments shown by Bom et al. (2005b) the vehicle speeds are set to 1 m/s and the results are shown for a duration less than 190 s. A decentralized control strategy, supported by inter-vehicle communications and relying on RTK GPS for localization, is also presented by Avanzini et al. (2009) for a vehicle-following system. Experiments were performed on four vehicles on a 240 m test path at a constant speed of 1 m/s. The maximum lateral deviation is observed to be -0.14 m and the maximum longitudinal error is observed to be 0.24 m.

1.7 Contributions of the Thesis

A list of novel contributions that have resulted from this thesis is presented below.

1. A framework for extending the VT&R method to a vehicle convoy.

2. A technique for modeling the concept of the VT&R method for controlling the inter-vehicle distance in a convoy.

3. A mathematical analysis showing that the longitudinal inter-vehicle distances are bounded and the bounds are independent of the number of the vehicles.

4. Design of a longitudinal distributed control law so that the leader does not need to be in the camera view of the followers.

1.8 Overview of the Thesis

Chapter 2 begins with a detailed background for designing a one dimensional spacing controller by using the concept of VT&R. The vehicle model used for designing the longitudinal controller in 1D is presented next. This is followed by a detailed description of the longitudinal control law along with a block diagram of the longitudinal controller. A mathematical analysis showing that the inter-vehicle distances are bounded and the bounds are independent of the number of the vehicles. This chapter ends with simulation results validating the design of the controller.

Chapter 3 provides a framework for combining the proposed longitudinal controller in 1D with a path tracker. A description of the vehicle model used in the path tracker is included. A detailed design of the path tracker is presented next, along with a block diagram of the lateral controller for the lateral and heading errors. This is followed by a block diagram of the combined lateral and longitudinal controllers. Simulation results are presented next to test the designed controllers. Conclusions and future work are presented in Chapter 4.

Chapter 2

The Longitudinal Controller in 1D

This chapter provides a detailed description of a one-dimensional spacing control problem. We study a very idealized situation where the vehicles are modeled as kinematic integrators. A detailed design of the longitudinal controller for controlling the inter-vehicle distance in 1D is presented. In addition, a block diagram of the system architecture is also provided, along with simulation results to validate the design of the controller.

2.1 Problem Formulation

Consider $(N + 1)$ vehicles moving along a 1D path, that is, along a straight line. They form a convoy with one manually-driven leader and N autonomous followers. Each vehicle is equipped with wheel encoders and a monocular camera, and has computational capability. A vision-based vehicle-following system has already been studied by Goi et al. (2010), where each vehicle can see the one in front. Here, we relax this assumption, but allow the vehicles to communicate with each other. For incorporating the concept of VT&R, we further postulate that there are landmarks that can be used for building maps. In particular, we take the very idealized situation that there is a hill that can be seen by all the vehicles as shown in Figure 2.1. This serves as a simple model of the vision-based localization system used in the VT&R method. It is further assumed that

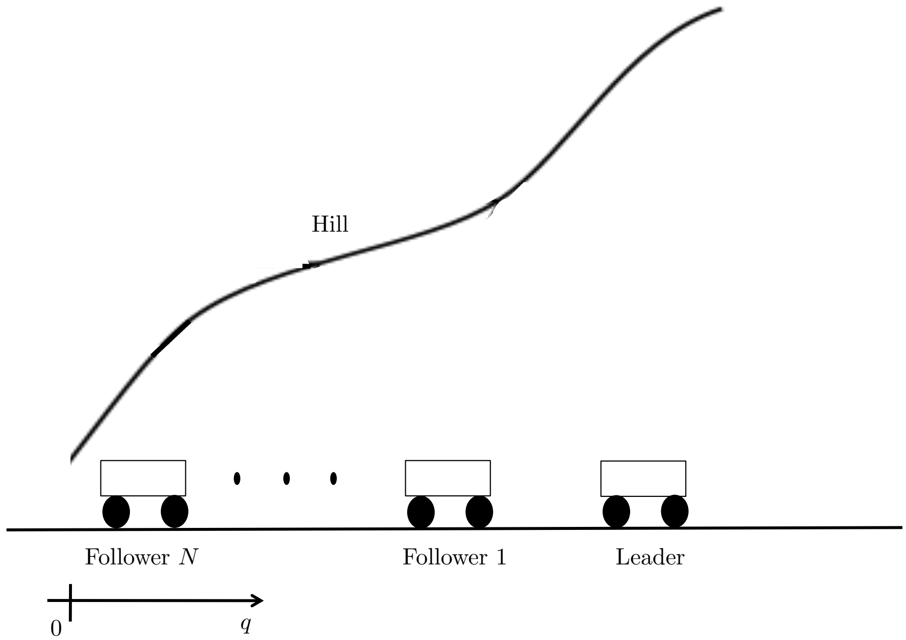

Figure 2.1: A convoy of inter-communicating vehicles moving in 1D. A hill is considered in the background that can be seen by all the vehicles. The hill's profile is assumed to be a captured by a function $h(q)$ and each vehicle stores the h values, which are used as landmarks.

the hill's profile is captured by a function $h(q)$, where q is the distance from the starting point of the convoy and h is a possibly unknown monotonically increasing function of q as shown in Figure 2.2. This assumption ensures that $h(q)$ has a unique value for every q. We take $h(q)$ to be the height of the hill as a function of the distance from the starting point of the convoy. The wheel encoders measure the current speed and the camera measures the elevation of the hill. As the vehicles travel, each vehicle stores the h values, which are used as landmarks. As these landmarks are uniquely determined for all values of q, the vehicles can localize themselves using a vision-based localization system. Thus, the landmarks can be used by the vehicles for map building as required in the VT&R method. As our setup is in 1D only, the goal of a follower is to maintain a desired distance with respect to the leader with the help of inter-vehicle communications.

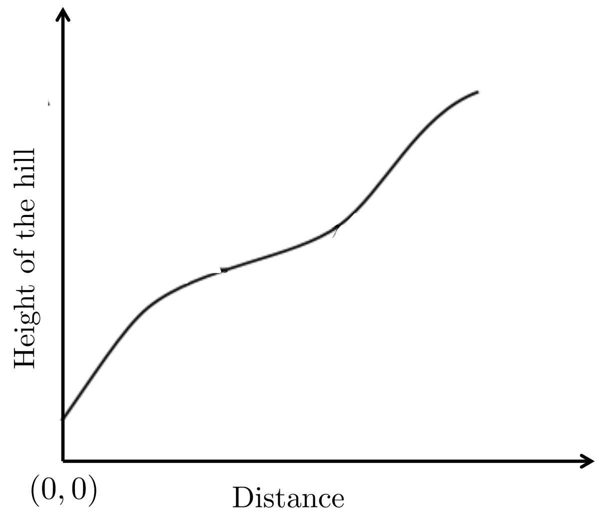

Figure 2.2: Example of a h function.

2.2 Vehicle Model

All signals are at time t unless otherwise stated.

By referring to the explanation of Figure 1.4 given in Section 1.2, we take a simple kinematic model for each vehicle. In control engineering, the motion of the i^{th} vehicle is written as

$$\dot{q}_i = u_i,$$

where q_i is the position and u_i is the velocity command input. The measured velocity is denoted, for example, by $\hat{u}_i$. In robotics, however, the equation is written as

$$\dot{q}_i = u_i + \varepsilon_i,$$

where u_i is the measured velocity. So, $u_i + \varepsilon_i$ is the commanded velocity, q_i is the actual position of the i^{th} vehicle with respect to the starting point of the convoy, and ε_i is a bounded sensor noise. Similarly, the measured value of the hill's elevation by the camera is modelled by

$$l_i = h(q_i) + \eta_i,$$

where η_i is a bounded sensor noise. The equations modeling the i^{th} vehicle are therefore

$$\dot{q}_i = u_i + \varepsilon_i \tag{2.1}$$

$$l_i = h(q_i) + \eta_i, \tag{2.2}$$

where $i = 0$ denotes the leader, and $i \in \{1, 2, \dots, N\}$ denotes the i^{th} follower. Henceforth, the subscript i runs over the set $\{1, 2, \dots, N\}$. Based on the above kinematic model, we designed a longitudinal controller. The next section examines the controller design.

2.3 Design of the Longitudinal Controller

The leader estimates its position by integrating the measured velocity, that is, it dead reckons:

$$\hat{q}_0(t) = \int_0^t u_0(\tau) d\tau, \quad \hat{q}_0(0) = 0. \tag{2.3}$$

The goal is to have $q_0 - q_i = r_{\text{des},i}$, where $r_{\text{des},i} > 0$ is the distance between the leader and the i^{th} follower. Therefore, the longitudinal error is defined as

$$e_{0i} = q_0 - q_i - r_{\text{des},i}. \tag{2.4}$$

Now we define t_i implicitly via

$$q_0(t_i) = q_0(t) - r_{\text{des},i}, \tag{2.5}$$

that is, t_i, which is a function of t, is the exact prior time when the leader was distance $r_{\text{des},i}$ behind its current actual position. As the function $h(q)$ is assumed to be monotonically increasing, a unique value of $h\big(q_0(t_i)\big)$ is obtained for each $q_0(t_i)$. Thus, t_i is uniquely determined by the measurement of $h\big(q_0(t_i)\big)$. If $h(q)$ is not assumed to be a monotonically increasing function, then more than one value of q_0 can be assigned to particular value of $h(q_0)$ leading to multiple values of t_i for a particular measurement of the hill's elevation. The exact t_i is not known to any of the vehicles. Since the leader cannot calculate its actual position at time t, we define an estimate of t_i, $\hat{t}_i$, implicitly via

$$\hat{q}_0(\hat{t}_i) = \hat{q}_0(t) - r_{\mathrm{des},i}. \tag{2.6}$$

From (2.3) and (2.6) we get

$$r_{\mathrm{des},i} = \int_{\hat{t}_i}^{t} u_0(\tau)d\tau. \tag{2.7}$$

We define the bounded signals

$$\varepsilon_{0i} = \varepsilon_0 - \varepsilon_i \tag{2.8}$$

$$\eta_{i0} = \eta_i - \eta_0(\hat{t}_i). \tag{2.9}$$

Finally, the desired control law for the i^{th} vehicle is taken to be

$$u_i = u_0 + k_i\big(l_0(t_i) - l_i\big), \tag{2.10}$$

where k_i is a positive gain. In order to implement this control law, we can use only those signals that are measurable at time t. Table 2.1 lists all the measurable and nonmeasurable signals that are being used in the model. Thus, the implemented control

Signals	Measurable
q_i	No
u_i	Yes
l_i	Yes
$h(q_i)$	No
$\hat{q}_i$	Yes
t_i	No
$\hat{t}_i$	Yes

Table 2.1: Measurable and nonmeasurable signals.

law is taken to be

$$
\begin{aligned}
u_i &= u_0 + k_i\big(l_0(\hat{t}_i) - l_i\big) && && (2.11)\\
&= u_0 + k_i\Big(h\big(q_0(\hat{t}_i)\big) + \eta_0(\hat{t}_i) - h(q_i) - \eta_i\Big). && \text{from (2.2)} && (2.12)
\end{aligned}
$$

Starting with (2.7), we have

$$
\begin{aligned}
r_{\mathrm{des},i} &= \int_{\hat{t}_i}^{t} u_0(\tau)d\tau \\
&= \int_{\hat{t}_i}^{t} \Big(\dot{q}_0(\tau) - \varepsilon_0(\tau)\Big)d\tau && \text{from (2.1)} \\
&= q_0 - q_0(\hat{t}_i) - \int_{\hat{t}_i}^{t} \varepsilon_0(\tau)d\tau. && \text{by integration} && (2.13)
\end{aligned}
$$

This implies that

$$
q_0(\hat{t}_i) = q_0 - r_{\mathrm{des},i} - \int_{\hat{t}_i}^{t} \varepsilon_0(\tau)d\tau. \tag{2.14}
$$

Substituting (2.14) into (2.12) yields

$$
u_i = u_0 + k_i\left(h\left(q_0 - r_{\mathrm{des},i} - \int_{\hat{t}_i}^{t} \varepsilon_0(\tau)d\tau\right) + \eta_0(\hat{t}_i) - h(q_i) - \eta_i\right). \tag{2.15}
$$

Let

$$
w_i = \int_{\hat{t}_i}^{t} \varepsilon_0(\tau)d\tau. \tag{2.16}
$$

Then from (2.15) we get

$$
u_i = u_0 + k_i\big(h(q_0 - r_{\mathrm{des},i} - w_i) + \eta_0(\hat{t}_i) - h(q_i) - \eta_i\big). \tag{2.17}
$$

Table 2.2 summarizes all the relevant equations used in the model.

For the system modeled by the equations in Table 2.2, we take the state to be

$$
\begin{bmatrix} x_0 \\ x_i \end{bmatrix} = \begin{bmatrix} q_0 - r_{\mathrm{des},i} \\ q_i \end{bmatrix}. \tag{2.18}
$$

	Equations
Leader	$\dot{q}_0 = u_0 + \varepsilon_0$ $l_0 = h(q_0) + \eta_0$
i^{th} follower	$\dot{q}_i = u_i + \varepsilon_i$ $l_i = h(q_i) + \eta_i$
$\hat{t}_i$	$r_{\text{des},i} = \int_{\hat{t}_i}^{t} u_0(\tau) d\tau$
Control law for the i^{th} follower	$u_i = u_0 + k_i \Big(h\left(q_0 - r_{\text{des},i} - w_i\right)$ $+ \eta_0(\hat{t}_i) - h(q_i) - \eta_i \Big)$
Longitudinal error	$e_{0i} = q_0 - q_i - r_{\text{des},i}$

Table 2.2: Summary of the equations used in the model.

Then from (2.17) we get

$$
\begin{aligned}
u_i &= u_0 + k_i\big(h\left(x_0 - w_i\right) + \eta_0(\hat{t}_i) - h(x_i) - \eta_i\big) \\
&= u_0 + k_i\big(h\left(x_0 - w_i\right) - h(x_i)\big) + k_i\eta_0(\hat{t}_i) - k_i\eta_i
\end{aligned}
$$

$$= u_0 + k_i\big(h\,(x_0 - w_i) - h(x_i)\big) - k_i\eta_{i0}. \qquad \text{from (2.9)} \qquad (2.19)$$

Thus, the state and error equations are

$$\dot{x}_0 = u_0 + \varepsilon_0 \qquad \text{from (2.1) and (2.18)} \qquad (2.20)$$

$$\dot{x}_i = u_0 + k_i\big(h(x_0 - w_i) - h(x_i)\big) - k_i\eta_{i0} + \varepsilon_i \qquad \text{from (2.1), (2.18) and (2.19)} \qquad (2.21)$$

$$e_{0i} = x_0 - x_i. \qquad \text{from (2.4) and (2.18)} \qquad (2.22)$$

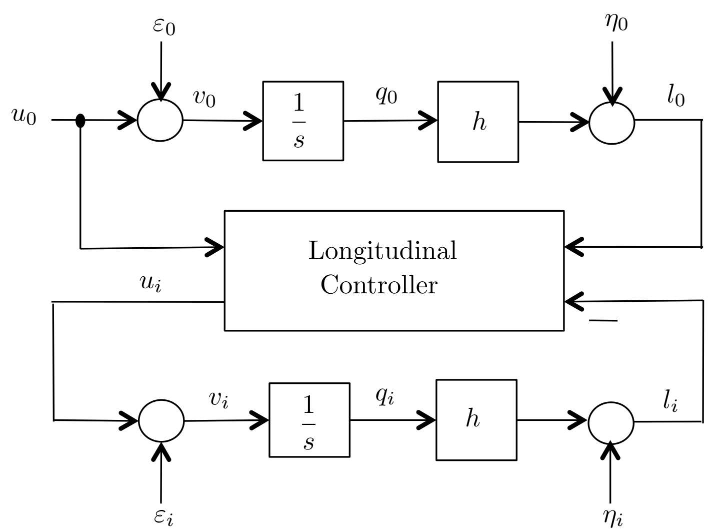

Figure 2.3: Block diagram of the longitudinal controller for the leader and i^{th} follower.

The block diagram of the longitudinal controller for the leader and the i^{th} follower is shown in Figure 2.3. We observe that the follower is referencing only the leader and has no communication with other followers. Thus, the equations modeling the followers are decoupled.

To study the dynamics of the error, e_{0i}, we consider the special case when $h(q_i) = aq_i$, where a is a positive real number that is unknown to the vehicles. From (2.22) the error dynamics equation is

$$
\begin{aligned}
\dot{e}_{0i} &= \dot{x}_0 - \dot{x}_i \\
&= -k_i\big(h(x_0 - w_i) - h(x_i)\big) + k_i\eta_{i0} + \varepsilon_{0i} && \text{from (2.20) and (2.21)} \\
&= -k_i\big(h(q_0 - r_{\text{des},i} - w_i) - h(q_i)\big) + k_i\eta_{i0} + \varepsilon_{0i} && \text{from (2.18)} \\
&= -k_i\Big(h\big(q_0(\hat{t}_i) - h(q_i)\big)\Big) + k_i\eta_{i0} + \varepsilon_{0i} && \text{from (2.13) and (2.16)} \\
&= -ak_i\big(q_0(\hat{t}_i) - q_i\big) + k_i\eta_{i0} + \varepsilon_{0i} && \text{using } h(q_i) = aq_i \\
&= -ak_i\big(q_0 - r_{\text{des},i} - w_i - q_i\big) + k_i\eta_{i0} + \varepsilon_{0i} && \text{from (2.14) and (2.16)} \\
&= -ak_i(x_0 - x_i) + ak_iw_i + k_i\eta_{i0} + \varepsilon_{0i} && \text{from (2.18)} \\
&= -ak_ie_{0i} + ak_iw_i + k_i\eta_{i0} + \varepsilon_{0i} && \text{from (2.22)} \qquad (2.23) \\
&= -ak_ie_{0i} + \alpha_i, && (2.24)
\end{aligned}
$$

where α_i is defined by

$$
\begin{aligned}
\alpha_i &= ak_iw_i + k_i\eta_{i0} + \varepsilon_{0i} && (2.25) \\
&= ak_i\left(\int_{\hat{t}_i}^{t} \varepsilon_0(\tau)d\tau\right) + k_i\eta_{i0} + \varepsilon_{0i}. && \text{from (2.16)}
\end{aligned}
$$

Note that (2.24) describes a BIBO stable system. If $\alpha_i(t)$ is bounded, then $e_{0i}(t)$ is bounded.

Theorem 1. *Consider the system modeled in Figure 2.3. Let the desired inter-vehicle spacing be $r_{des,\,i} > 0$ and let the h function be $h(q_i) = aq_i$, where a is a positive real number unknown to the vehicles. Assume that $\forall i$, the noises, $\varepsilon_i(t)$ and $\eta_i(t)$, are bounded signals and the norms, $\|\varepsilon_i\|_\infty$ and $\|\eta_i\|_\infty$, are bounded by values independent of N, the number of vehicles. Let the magnitudes of the initial errors, $|e_{0i}(0)|$, be bounded by a number, κ, independent of N. Assume that $u_0(t)$ is bounded below by a positive number, i.e.,*

$$(\exists\gamma > 0)(\forall t \geq 0)(u_0(t) \geq \gamma).$$

Then, the errors, $e_{0i}(t)$, are bounded and the norms, $\|e_{0i}\|_\infty$, are bounded by a number independent of N.

Proof. Let

$$\|\varepsilon_i\|_\infty \leq \zeta \qquad \text{by assumption} \tag{2.26}$$

and

$$\|\eta_i\|_\infty \leq \mu. \qquad \text{by assumption} \tag{2.27}$$

Since $u_0(t) \geq \gamma > 0$, therefore from (2.7) we get

$$\begin{aligned} r_{\text{des},i} &\geq \gamma \int_{\hat{t}_i(t)}^{t} d\tau \\ &= \big(t - \hat{t}_i(t)\big)\gamma. \qquad \text{by integration} \end{aligned}$$

Thus

$$\big(t - \hat{t}_i(t)\big) \leq \frac{r_{\text{des},i}}{\gamma}. \tag{2.28}$$

From (2.16)

$$\begin{aligned} |w_i(t)| &= \left| \int_{\hat{t}_i(t)}^{t} \varepsilon_0(\tau) d\tau \right| \\ &\leq \big(t - \hat{t}_i(t)\big) \|\varepsilon_0\|_\infty \\ &\leq \frac{r_{\text{des},i}}{\gamma}\zeta. \qquad \text{from (2.26) and (2.28)} \end{aligned}$$

Since the right-hand side is independent of t,

$$\|w_i\|_\infty \leq \frac{r_{\text{des},i}}{\gamma}\zeta. \tag{2.29}$$

The error dynamics equation is

$$\dot{e}_{0i}(t) = -ak_i e_{0i}(t) + ak_i w_i(t) + k_i \eta_{i0}(t) + \varepsilon_{0i}(t). \qquad \text{referring to (2.23)}$$

From (2.8), (2.9), and (2.29) we know that $\varepsilon_{0i}(t)$, $\eta_{i0}(t)$, and $w_i(t)$ are bounded signals. Hence, the errors, $e_{0i}(t)$, are bounded.

The solution of (2.24) with the initial condition, $e_{0i}(0)$, is

$$e_{0i}(t) = \exp(-ak_i t)e_{0i}(0) + (g_i * \alpha_i)(t),$$

where $g_i(t)$ is the impulse response function. Then in terms of 1-norm of g_i and the ∞-norm of α_i,

$$\begin{aligned} |e_{0i}(t)| &\leq |\exp(-ak_i t)e_{0i}(0)| + \|g_i\|_1 \|\alpha_i\|_\infty \\ &\leq \kappa + \|g_i\|_1 \|\alpha_i\|_\infty . \end{aligned} \tag{2.30}$$

We know

$$\begin{aligned} |\alpha_i(t)| &= |ak_i w_i(t) + k_i \eta_{i0}(t) + \varepsilon_{0i}(t)| && \text{from (2.25)} \\ &= |ak_i w_i(t) + k_i \Big(\eta_i(t) - \eta_0\big(\hat{t}_i(t)\big)\Big) + \varepsilon_0(t) - \varepsilon_i(t)| && \text{from (2.8) and (2.9)} \\ &\leq ak_i |w_i(t)| + k_i |\eta_i(t)| + k_i |\eta_0\big(\hat{t}_i(t)\big)| + |\varepsilon_0(t)| + |\varepsilon_i(t)| \\ &\leq ak_i \|w_i\|_\infty + k_i \|\eta_i\|_\infty + k_i \|\eta_0\|_\infty + \|\varepsilon_0\|_\infty + \|\varepsilon_i\|_\infty \\ &\leq \frac{ak_i r_{\text{des},i}}{\gamma}\zeta + 2k_i\mu + 2\zeta && \text{by (2.26), (2.27), and (2.29)} \\ &\leq \left(2 + \frac{ak_i r_{\text{des},i}}{\gamma}\right)\zeta + 2k_i\mu. \end{aligned}$$

Since the right-hand side is independent of t,

$$\|\alpha_i\|_\infty \leq \left(2 + \frac{ak_i r_{\text{des},i}}{\gamma}\right)\zeta + 2k_i\mu. \tag{2.31}$$

Also

$$\|g_i\|_1 = \int_0^\infty |\exp(-ak_i t)|dt = \frac{1}{ak_i}. \tag{2.32}$$

Substituting (2.31) and (2.32) into (2.30) gives

$$|e_{0i}(t)| \leq \kappa + \left(\frac{2}{ak_i} + \frac{r_{\text{des},i}}{\gamma}\right)\zeta + \frac{2\mu}{a}.$$

Since the right-hand side is independent of t,

$$\|e_{0i}\|_\infty \leq \kappa + \left(\frac{2}{ak_i} + \frac{r_{\text{des},i}}{\gamma}\right)\zeta + \frac{2\mu}{a}. \tag{2.33}$$

Thus, $\|e_{0i}\|_\infty$ are bounded by a value that is independent of N. □

The following section examines the simulation model and the simulation results obtained by implementing the longitudinal controller in 1D.

2.4 Simulation Model

In order to validate our controller model, we created a simulation environment in MATLAB. In the simulation algorithm we have bounded the lower limit of the control speed u_i to 0. This ensures that for the time period when the leader has not travelled forward a distance $r_{\text{des},i}$, the follower stays at its initial position and does not move backwards. The simulation block diagram for the leader and the i^{th} follower is shown in Figure 2.4. The following pseudocode shows how the longitudinal controller block works:

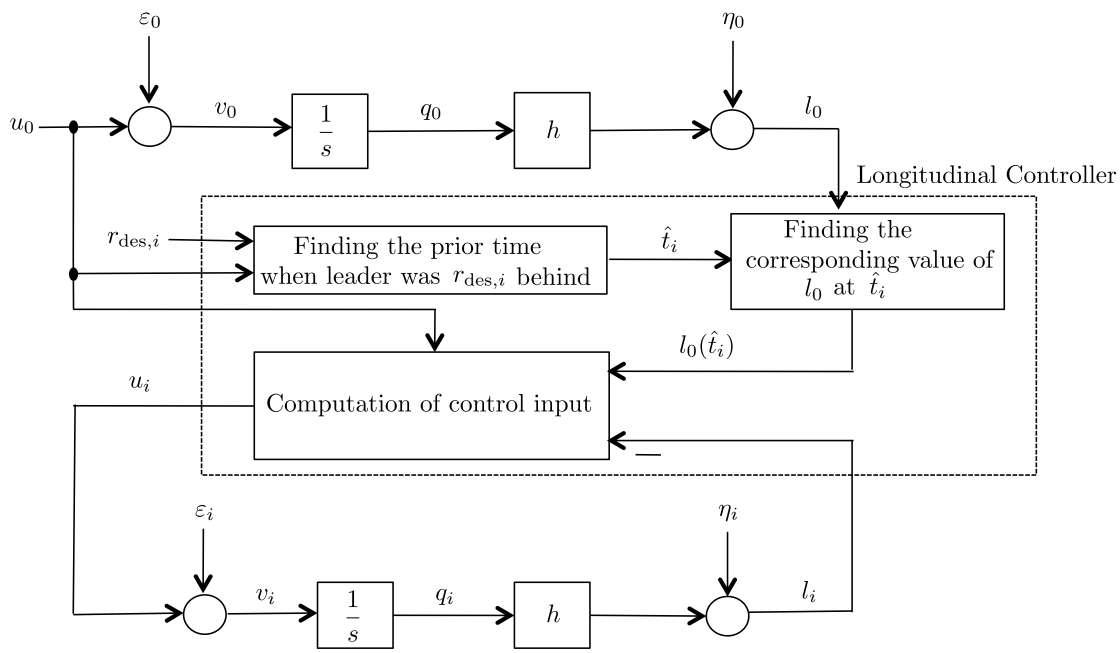

Figure 2.4: Simulation block diagram of the longitudinal controller.

while the leader communicates u_0 and l_0 **do**

  if $l_0 \geq ar_{\text{des},i}$ **then**

    Store l_0 and read in l_i.

    Calculate $\hat{t}_i$ by using (2.7).

    Calculate $l_0(\hat{t}_i)$ by using a search algorithm.

    Calculate the control speed by using (2.11) and apply it to the follower.

  else

    $u_i = 0$.

  end if

end while

2.4.1 System Parameters

The controller design was aimed to be tested on Roombas. Thus, the leader's speed was chosen so as to be compatible with the Roomba's specification. Roomba's optimal speed range is 0.1 m/s - 0.8 m/s. We chose the leader's speed to be 0.3 m/s. In order to account for noise measurements, a tolerance of ±0.05 m/s is specified on the speed measurement. Thus, the maximum allowable speed of all the vehicles is set to 0.8 ±0.05 m/s. The measured speed of the vehicles and output of the h function are corrupted by zero-mean white Gaussian noises.

For the longitudinal controller, the configurable parameter is the controller gain k_i. A detailed illustration of the computation of the control input for $h(q_i) = aq_i$ is shown in Figure 2.5. The closed-loop transfer function for reference input $l_0(\hat{t}_i)$ changes is

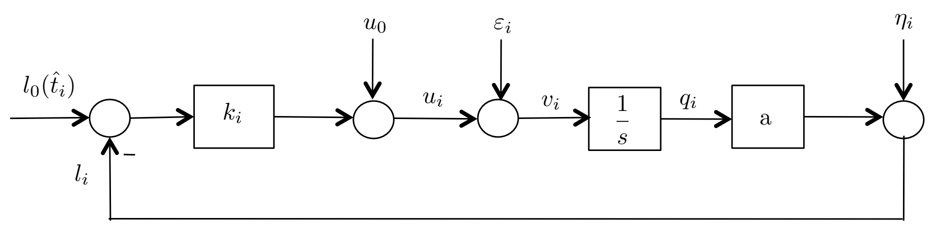

Figure 2.5: Block diagram of the control input of an i^{th} follower.

$$\frac{1}{\tau s + 1}, \tag{2.34}$$

where $\tau = \frac{1}{ak_i}$. Thus, the gain, k_i, is calculated by specifying a desired τ. We took the desired τ to be 10 s. Accordingly, k_i was set at 0.02. Table 2.3 summarizes all the variables used in the controller design along with the values used in the simulation.

Simulations were performed for the block diagram shown in Figure 2.4 with one and two followers to validate the controller design. The manually-driven leader was simulated by specifying a constant speed of 0.3 m/s. The leader and the follower positions at the start of the simulation were 0 m. All other parameters were taken as specified in Table 2.3. During the simulations it was observed that for a given τ, if the longitudinal error when the follower started to move was increased, then the speed of the follower exceeded the required specifications. In order to meet the speed requirements, the maximum allowable longitudinal error when the follower started to move was found to be 5 m by simulation.

Description	Symbol	Value
Measured speed of the leader	u_0	0.3 m/s
Process noise variance on speed	σ_u^2	4×10^{-6} m^2/s^2
Desired inter-vehicle distance	$r_{\text{des},i}$	6 m
$h(q_i)$ function	h	$5q_i$
Process noise variance on the measurement of h	σ_h^2	4×10^{-4} m^2
Longitudinal error gain	k_i	0.02

Table 2.3: Parameters used in the simulation model. The process noises are implemented as discrete-time signals in MATLAB.

In the following section, we present simulation results for the following two different scenarios: (S_1) The longitudinal error when the follower starts to move is 0 m and (S_2) The longitudinal error when the follower starts to move is 5 m. In both cases, the root mean square (rms) value of the longitudinal error is calculated from the time when the follower starts to move.

2.4.2 Simulation Results

One follower

1. In this case, when the follower starts to move, the leader has travelled a distance of 6 m. Thus, the longitudinal error when the follower starts to move is 0 m. The results are shown in Figure 2.6. The output of the h function as measured by the leader is shown in Figure 2.6a. Figure 2.6b shows the trajectories of the leader and follower. Notice in Figure 2.6b that the follower remains at its initial position till 20 s as the leader has not travelled a distance of 6 m. Figure 2.6c shows the longitudinal error. The initial longitudinal error is -6 m and it increases to 0 m as

the leader travels. The rms value of the longitudinal error is 0.006 m. The leader's and follower's speeds are shown in Figure 2.6d.

2. Here, when the follower starts to move, the leader has travelled a distance of 11 m. Hence, the longitudinal error when the follower starts to move is 5 m. The results are shown in Figure 2.7. Notice in Figure 2.7b that when the follower starts to move its speed is 0.8 m/s, which is acceptable as per our specifications. As the longitudinal error is 5 m when the follower starts, therefore the rms value of longitudinal error is more than in S_1 and it is 0.888 m.

In the above plots, we were using a point integrator to model the vehicles. In order to account for some dynamics in the model, we added a first order lag $\frac{1}{\tau_c s+1}$ on the control speed, where τ_c is the time constant of the vehicle model. The block diagram of the model on adding the dynamics is shown in Figure 2.8. Simulations were performed for the two different cases as described in S_1 and S_2. The block diagram was taken as shown in Figure 2.4 but the follower was modeled as shown in Figure 2.8. All the parameters were taken as specified in Table 2.3 and τ_c was set to 5 s.

1. In this case, when the follower starts to move, the leader has travelled a distance of 6 m. Thus, the longitudinal error when the follower starts to move is 0 m. The results obtained are shown in Figure 2.9. Figure 2.9a shows the trajectories of the leader and follower. The longitudinal error is shown in Figure 2.9b. On comparing Figure 2.6c and Figure 2.9b, we observe that in Figure 2.9b the longitudinal error does not go to zero immediately due to the added dynamics in the model. The rms value of the longitudinal error is calculated to be 0.261 m. Figure 2.9c shows the leader's and follower's speeds. Notice in Figure 2.9c that the speed response of the model becomes sluggish.

2. The longitudinal error when the follower starts to move is 5 m. Simulation results are shown in Figure 2.10. Figure 2.10a shows the trajectories of the leader and

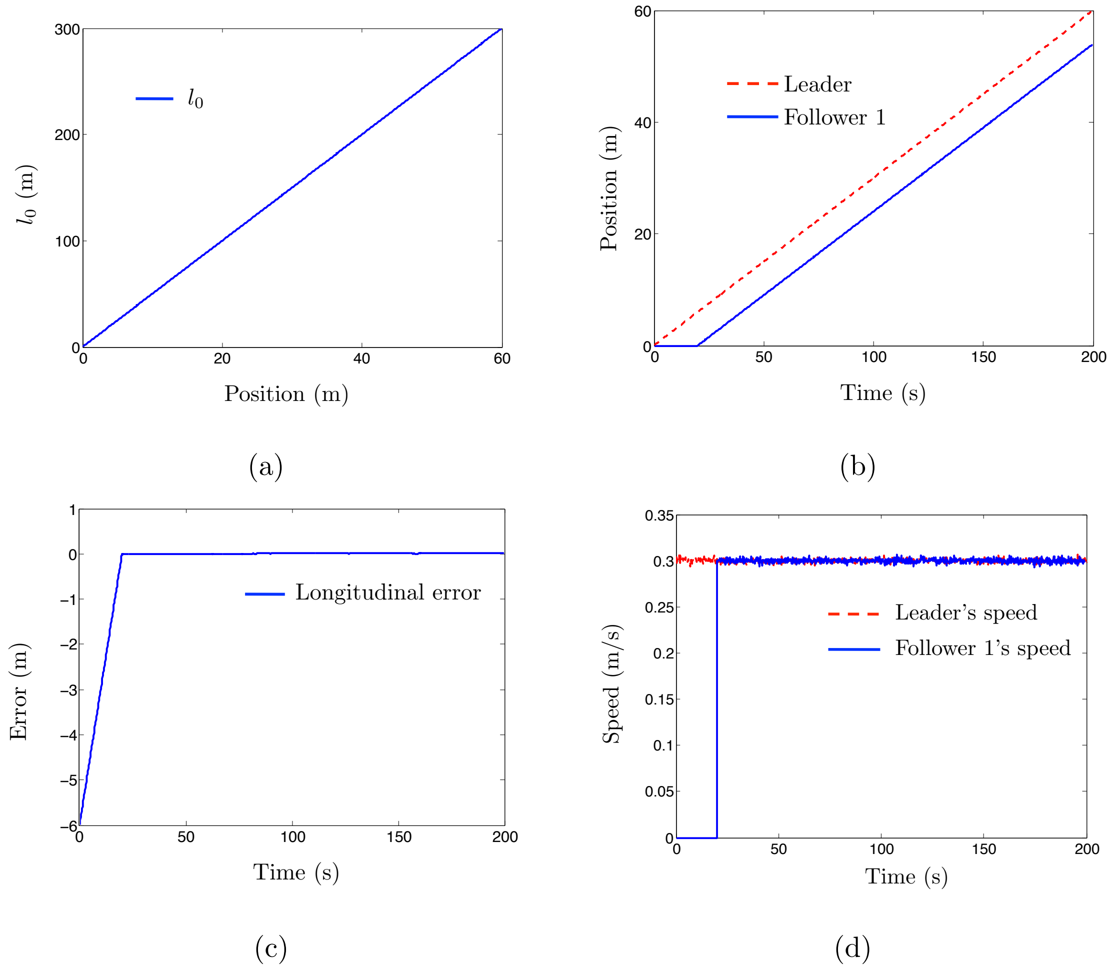

Figure 2.6: Simulated plot for $h(q_i) = 5q_i$ and the longitudinal error is 0 m when the follower starts: (a) l_0 as measured by the leader. (b) Leader's and follower's trajectories. (c) The longitudinal error. (d) Leader's and follower's speeds.

the follower. The longitudinal error is shown in Figure 2.10b. The rms value of the longitudinal error is calculated to be 1.324 m. The leader's and the follower's speeds are shown in Figure 2.10c. Results obtained are similar to the ones shown in Figure 2.9. Notice in Figure 2.10c that the speed of the follower is within the optimal range, that is, 0.1 m/s - 0.8 m/s.

Thus, we conclude that for the block diagram shown in Figure 2.4 and the parameters specified in Table 2.3, the speed specification is met if the longitudinal error is less than

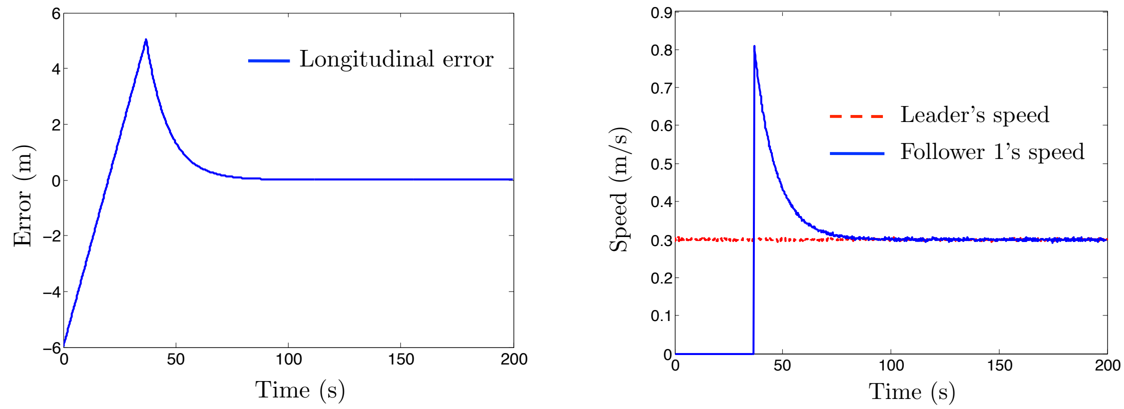

(a) (b)

Figure 2.7: Simulated plot for $h(q_i) = 5q_i$ and the longitudinal error is 5 m when the follower starts: (a) The longitudinal error. (b) Leader's and follower's speeds.

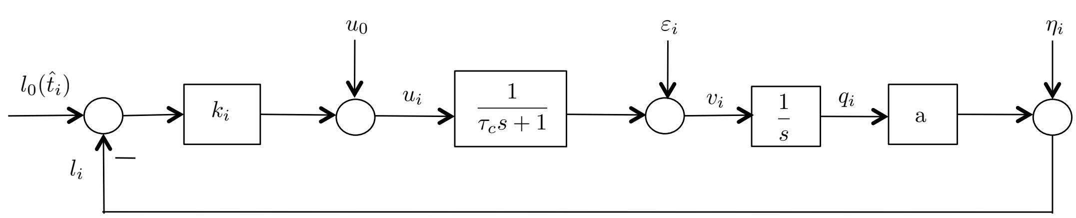

Figure 2.8: Block diagram of the control input with dynamics added to the follower model.

5 m when the follower starts to move. If the longitudinal error is increased to 5.5 m when the follower moves, then the speed specification is not met though the magnitude of longitudinal error remains bounded as shown in Figure 2.11.

Now we look at an affine $h(q_i)$ function, $h(q_i) = 5q_i+20$, and keep all other parameters as specified in Table 2.3. Simulations were performed for the block diagram shown in Figure 2.4 and the longitudinal error when the follower started to move was taken to be 0 m and 5 m. We take $k_1 = 0.02$ even though $h(q_i)$ is not a linear function. Results are shown in Figure 2.12 and Figure 2.13, respectively. Notice in Figure 2.12d and Figure 2.13b that the speed requirement is met. The longitudinal error remains bounded as seen

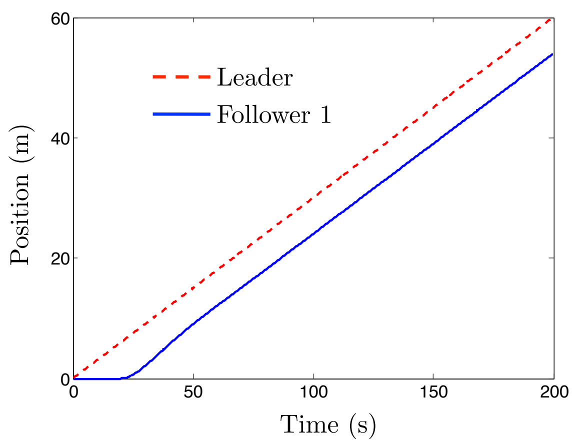

(a)

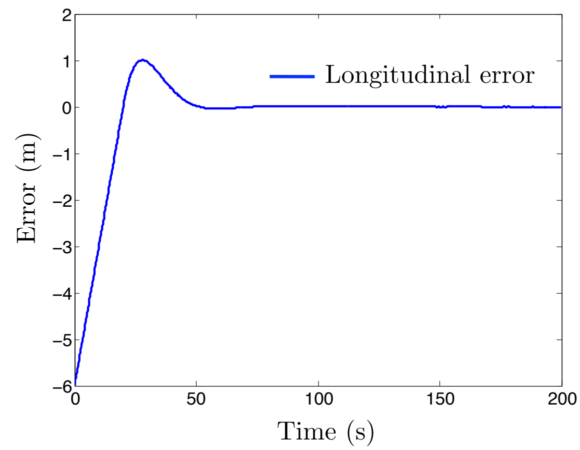

(b)

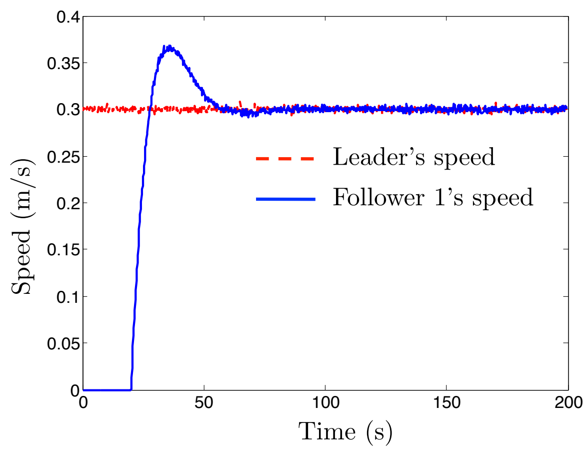

(c)

Figure 2.9: Simulated plot for $h(q_i) = 5q_i$, $\tau_c = 5$ s, and the longitudinal error is 0 m when the follower starts: (a) Leader's and follower's trajectories. (b) The longitudinal error. (c) Leader's and follower's speeds.

in Figure 2.12c and Figure 2.13a. Thus, the designed longitudinal controller worked well even when changing the $h(q_i)$ function.

Simulations were next performed on two followers to validate the controller design.

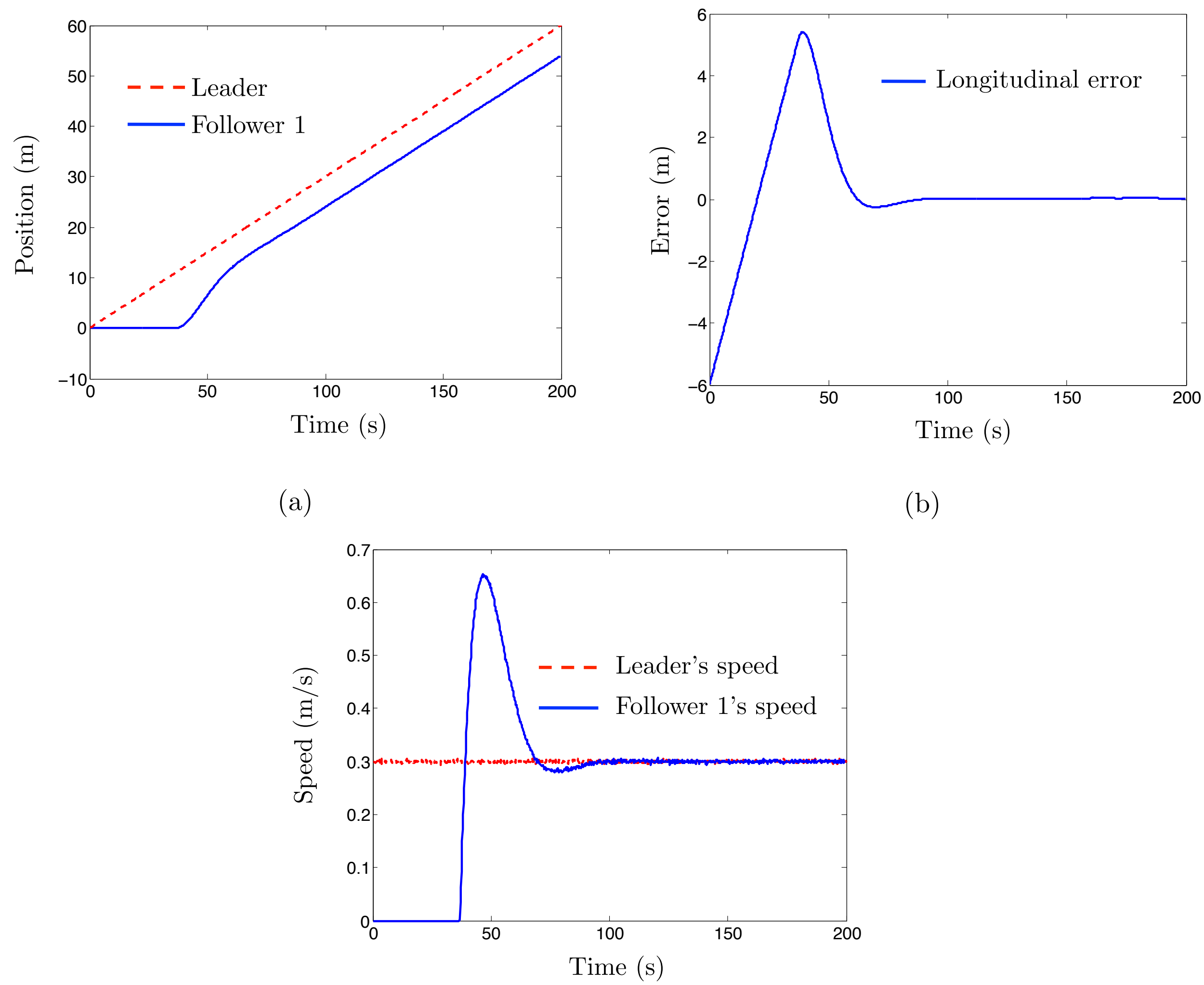

(a) (b)

(c)

Figure 2.10: Simulated plot for $h(q_i) = 5q_i$, $\tau_c = 5$ s, and the longitudinal error is 5 m when the follower starts: (a) Leader's and follower's trajectories. (b) The longitudinal error. (c) Leader's and follower's speeds.

Two Followers

With two followers, simulations were performed for the block diagram shown in Figure 2.4 but the follower model was taken as shown in Figure 2.8 so that we could observe the effect of dynamics too. The inter-vehicle distance was taken to be 6 m. Thus, $r_{\text{des},1} = 6$ m and $r_{\text{des},2} = 12$ m. We took $\tau_c = 5$ s while all the other parameters were taken as

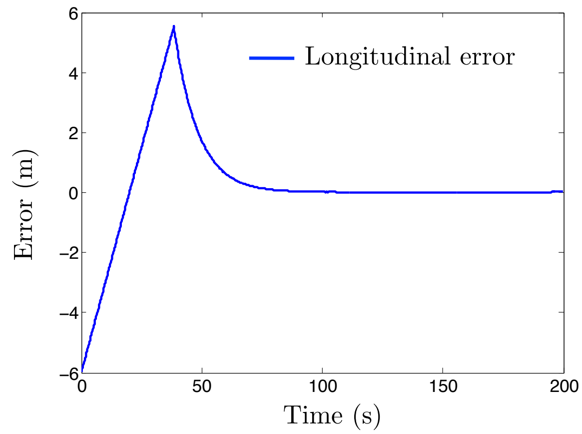

(a)

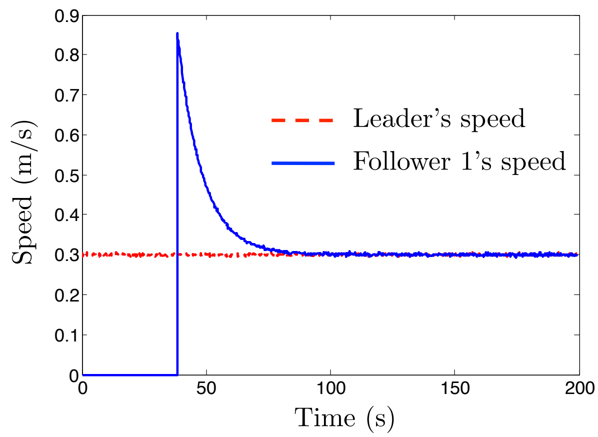

(b)

Figure 2.11: Simulated plot for $h(q_i) = 5q_i$ and the longitudinal error is 5.5 m when the follower starts: (a) The longitudinal error. (c) Leader's and follower's speeds.

specified in Table 2.3. The longitudinal errors when the followers start to move are 0 m. Figure 2.14a shows the trajectories of the leader and the two followers. The longitudinal errors are shown in Figure 2.14b. The leader's and the two follower's speeds are shown in Figure 2.14c. Both the followers show similar behaviors and the results are similar to the ones shown in Figure 2.9.

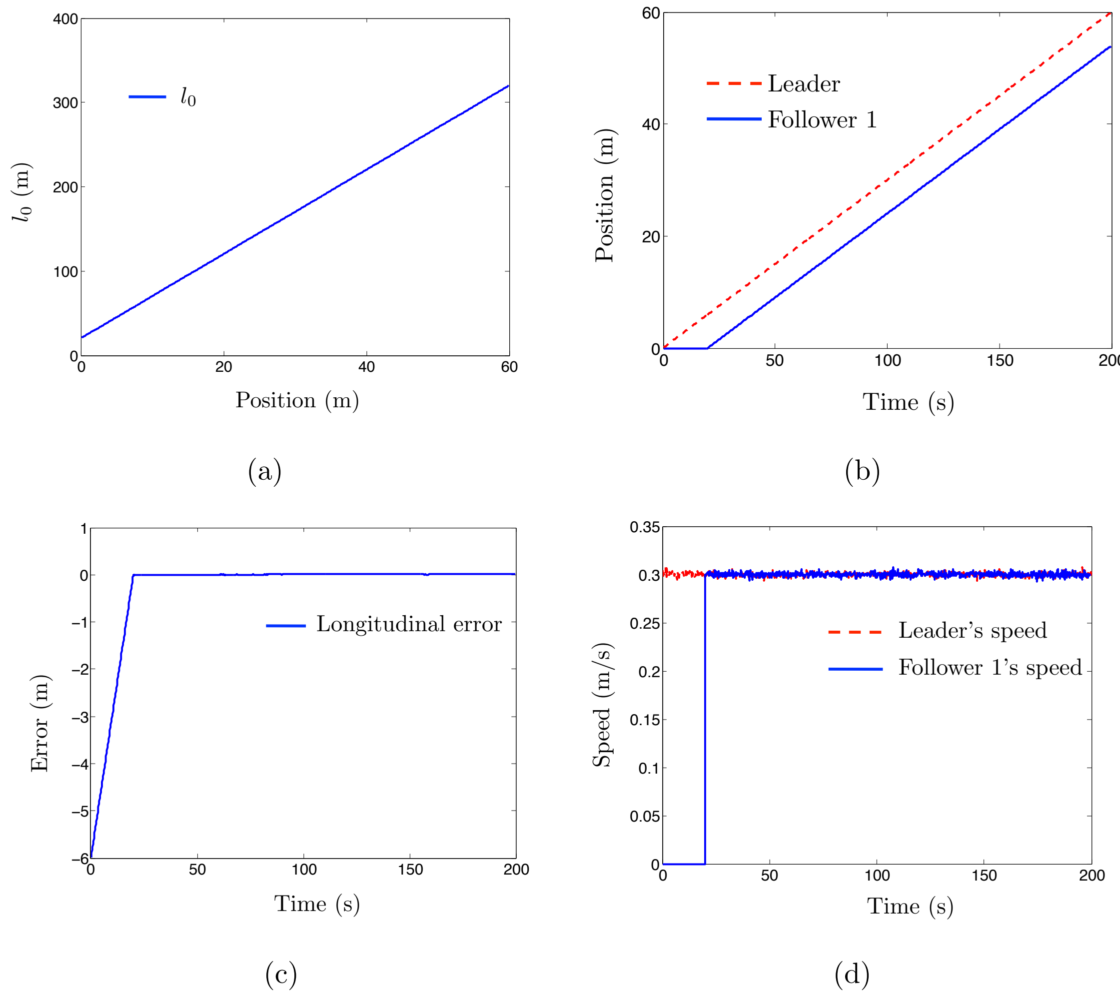

Figure 2.12: Simulated plot for $h(q_i) = 5q_i + 20$ and the longitudinal error is 0 m when the follower starts: (a) l_0 as measured by the leader. (b) Leader's and follower's trajectories. (c) The longitudinal error. (d) Leader's and follower's speeds.

2.5 Collision Problem

Consider the simulation result shown in Figure 2.14a. Here both the followers are referencing the leader only. So, they will collide with one another if the first follower stops as shown in Figure 2.14d. Hence, we need to take into consideration the inter-vehicle spacing too. So, we allow the $(i-1)^{\text{th}}$ follower to communicate the output of the $h(q)$ function, l_{i-1}, and its speed, u_{i-1}, to the i^{th} follower. A minimum inter-vehicle distance,

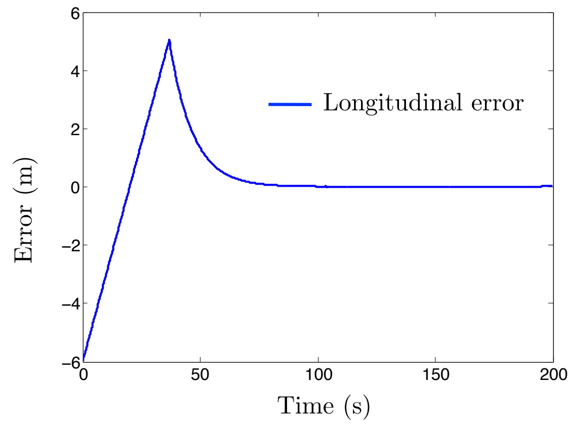

(a)

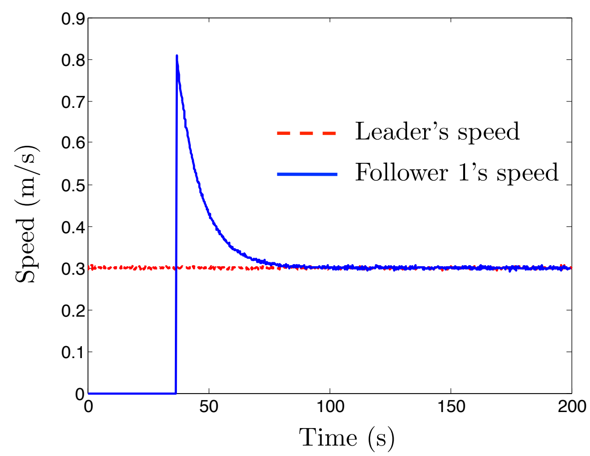

(b)

Figure 2.13: Simulated plot for $h(q_i) = 5q_i + 20$ and the longitudinal error is 5 m when the follower starts: (a) The longitudinal error. (b) Leader's and follower's speeds.

r_{danger}, is specified such that $\frac{r_{\text{des},i}}{r_{\text{danger}}} < 20$ to avoid a collision between two consecutive followers. In order to take into account the dynamics of the vehicles, a safety measure of 1.5 m is added to r_{danger}. This safety measure is determined by simulations. The safety measure value is obtained by increasing its value from 0 until the i^{th} vehicle stops without colliding with the $(i-1)^{\text{th}}$ follower. As we are measuring l_i's, so the minimum difference in the measurement of l_i's of two consecutive followers is set to $a(r_{\text{danger}} + 1.5)$. We refer to the controller designed as per Figure 2.4 as the old controller. As before, the speeds

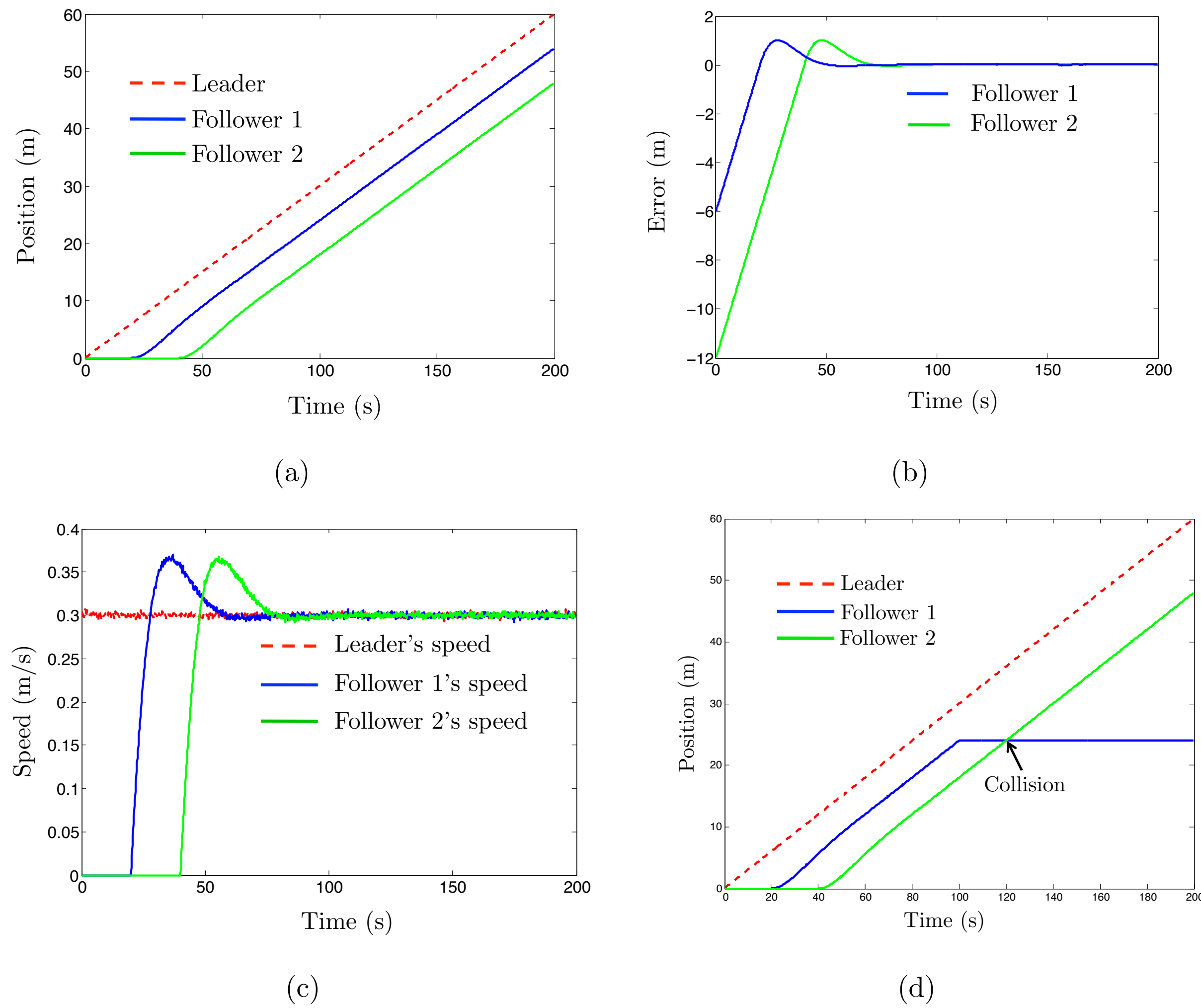

Figure 2.14: Simulated plot for $h(q_i) = 5q_i$, $\tau_c = 5$ s, and the longitudinal errors when the followers start are 0 m: (a) Leader's and follower's trajectories. (b) The longitudinal error. (c) Leader's and follower's speeds. (d) Occurrence of collision if the first follower stops.

of the followers are lower bounded by 0. For the i^{th} follower, a pseudocode for collision avoidance is given below.

while the leader communicates u_0 and l_0, and $(i-1)^{\text{th}}$ follower communicates u_{i-1} and l_{i-1} **do**

Store l_0 and l_{i-1} and read in l_i .

if $l_0 \geq ar_{\text{des},i}$ **then**

if $|l_i - l_{i-1}| > a(r_{\text{danger}} + 1.5)$ **then**

Follow the old controller code.

else

$u_i = u_{i-1} - 0.05$ and if $u_i < 0$, then u_i is set to 0.

end if

else

$u_i = 0.$

end if

end while

Figure 2.15 shows the simulation results obtained by implementing the above code on two followers modeled by the block diagram shown in Figure 2.4 but with the followers modeled as shown in Figure 2.8. We take $\tau_c = 5$ s, $k_i = 0.02$, $r_{\text{danger}} > 0.3$ m, $r_{\text{des},1} = 6$ m, and $r_{\text{des},2} = 12$ m. The first follower stops after travelling for a time duration of 100 s as shown in Figure 2.15a. The second follower starts to move when the leader has travelled a distance of 12 m as seen in Figure 2.15a. However, when the distance between the first and second followers reduces to less than $r_{\text{danger}} + 1.5$ m at about 130 s, the second follower's speed decreases even though the leader continues to move as seen in Figure 2.15c. Figure 2.15b shows a close-up of the trajectories of the leader and the follower. The spacing between the first and second followers is about 0.3 m.

Simulations were also performed for the situation when the first follower started to move again after stopping. Figure 2.16a shows the trajectories of the three vehicles. The first follower stops for a time duration of 40 s after travelling a distance of about 13.5 m. The second follower initially begins to move when the leader has travelled a distance of

12 m as seen in Figure 2.16a. However, when the distance between the first and second followers reduces, the second follower's speed decreases even though the leader continues to move as seen in Figure 2.16c. The second follower stops to move as the first follower is not moving with a inter-vehicle spacing of about 0.3 m between them as shown in Figure 2.16b. When the first follower starts to move again at about 120 s, the second follower also starts to move as seen in Figure 2.16b. It should be noted that when the first and second follower vehicles start to move after stopping, the longitudinal error for both vehicles is more than 5 m as the leader has not stopped. Therefore, the speeds of the follower vehicles exceed the required specifications as seen in Figure 2.16c.

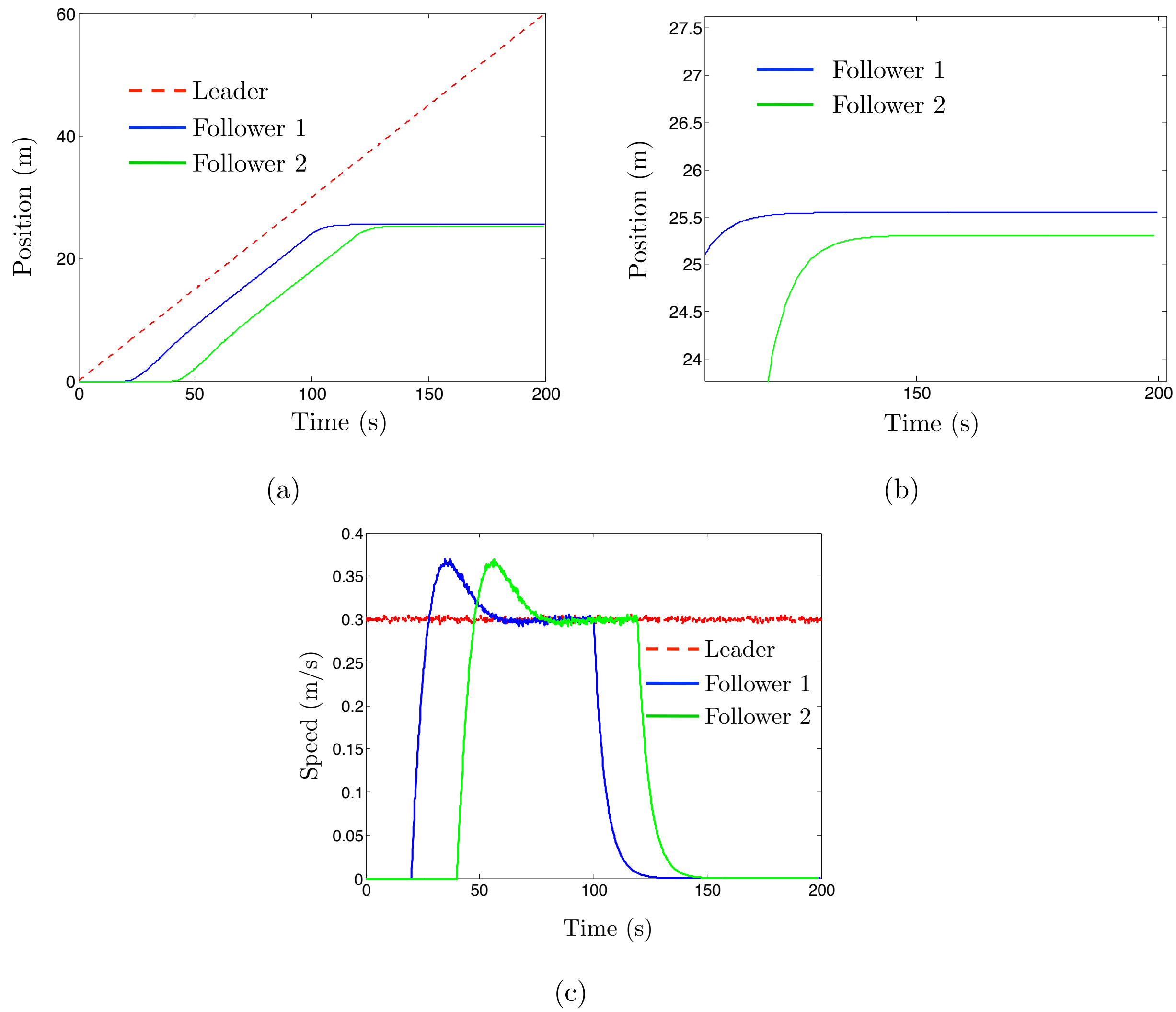

Figure 2.15: Simulated plots for the no collision case: (a) Leader's and the two follower's trajectories. (b) Close-up of the trajectories of the two followers. (c) Leader's and follower's speeds

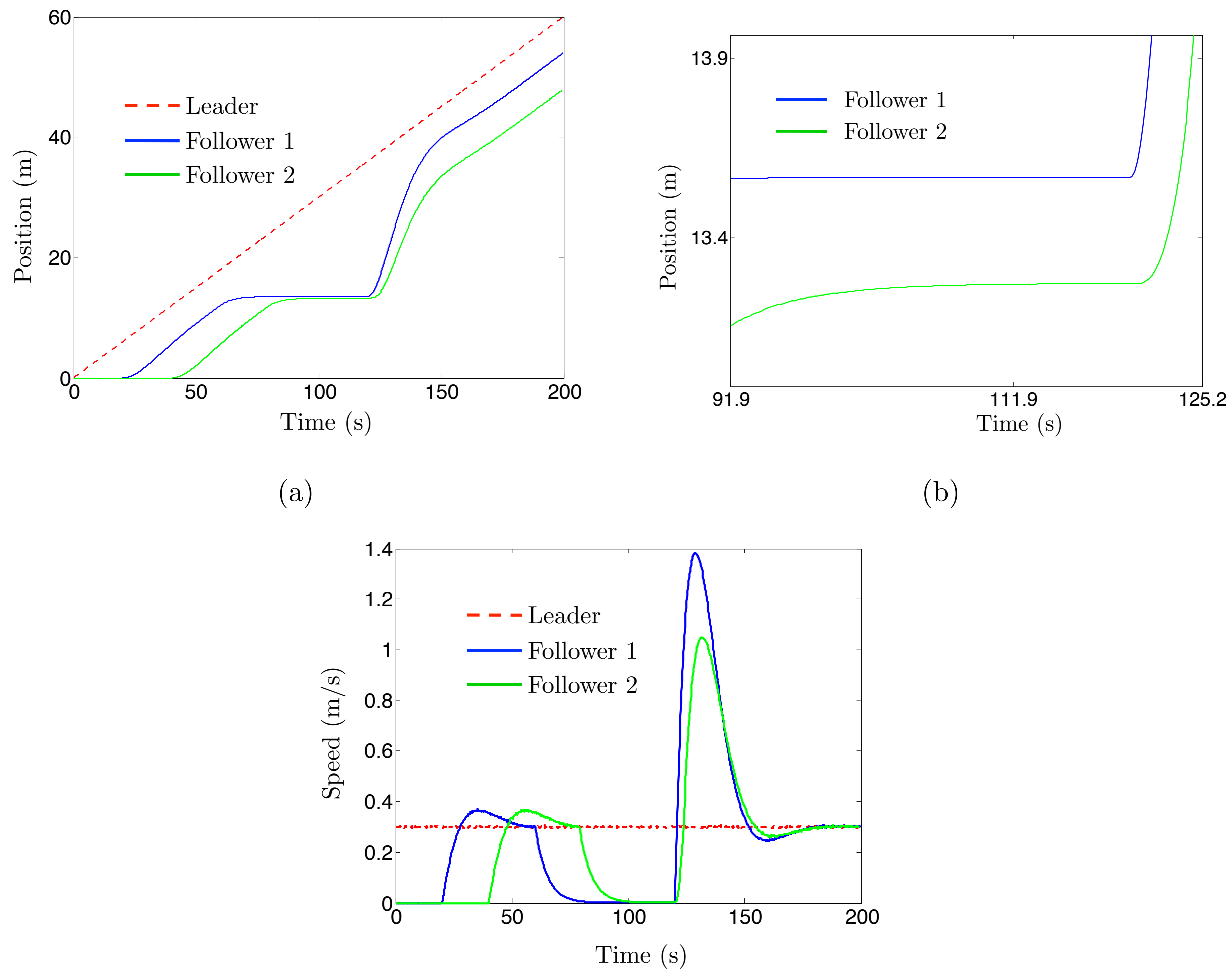

(c)

Figure 2.16: Simulated plots for the no collision case when the first follower starts to move again after stopping for some time: (a) Leader's and the two follower's trajectories. (b) Close-up of the trajectories of the two followers. (c) Leader's and follower's speeds.

Chapter 3

System Architecture and Design in 2D

This chapter examines the design of the path tracker in 2D. The aim is to implement the lateral controller for pathtracking and the longitudinal controller described in Chapter 2 for controlling the inter-vehicle spacing. A detailed block diagram for the combined lateral and longitudinal controller is also presented along with simulation results to validate the controller design.

3.1 Problem Formulation

The idea was to perform experiments with the Roomba robots available in the Autonomous Space Robotics Laboratory (ASRL) at University of Toronto Institute of Aerospace Studies (UTIAS). The testing was aimed to be done in the Vicon Lab at UTIAS, where the motion capture software called Vicon Nexus was to be used to provide high speed and high accuracy real-time tracking of vehicles. However, in the end, only simulations were performed for the above scenario.

The problem setup consists of $(N+1)$ inter-communicable wheeled robots moving in a GPS-like scenario that can be tested in the Vicon lab. Each vehicle has computational capability. They form a convoy with one manually-driven leader and N autonomous followers as shown in Figure 3.1. The goal of an autonomous follower is to track the

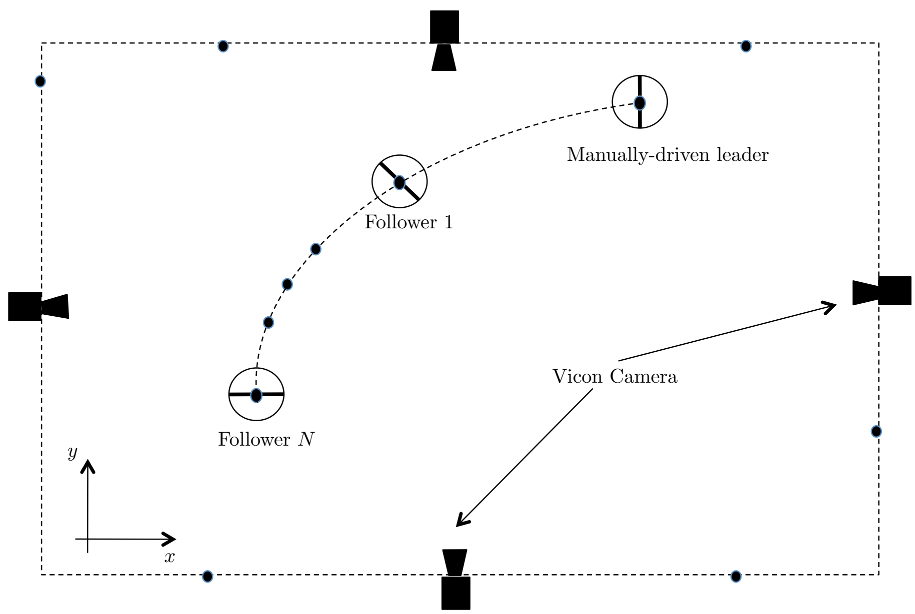

Figure 3.1: A vehicle convoy moving in the Vicon lab. The coordinate frame is attached to the Vicon system.

leader's path with a desired inter-vehicle spacing using the Vicon system for inter-vehicle communication. The block diagram of an autonomous follower with only lateral controller is shown in Figure 3.2. In the Vicon frame, the leader's position and heading are

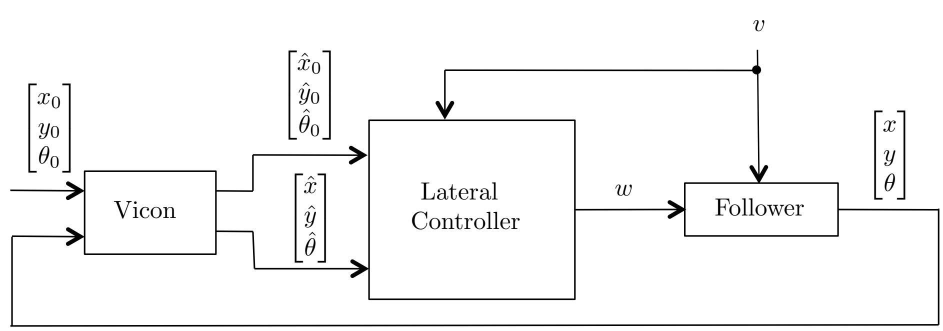

Figure 3.2: Block diagram of an autonomous follower with only lateral controller.

(x_0, y_0) and θ_0, respectively. Likewise, (x, y) and θ are the position and heading angle of the follower. Vicon outputs the measured leader's pose, $(\hat{x}_0, \hat{y}_0, \hat{\theta}_0)$, and the measured follower's pose, $(\hat{x}, \hat{y}, \hat{\theta})$, as expressed in the Vicon frame. The follower's speed, v, is assumed to be constant for now. These measurements are the inputs to the controller, which outputs the angular velocity, ω, to the follower. A detailed model of one of the followers is presented in the next section.

3.2 Vehicle Model

For modeling the follower's kinematics, we have used the unicycle model. Consider a point moving in a plane as shown in Figure 3.3. The state variables are the coordinates

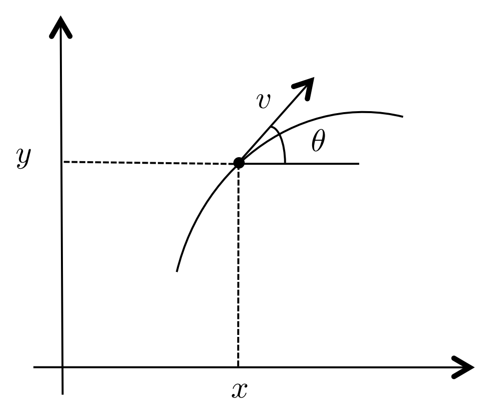

Figure 3.3: Unicycle model kinematics.

of the point, (x, y), and the heading angle, θ. The forward velocity of the moving point is v. The kinematic model equations of the unicycle are

$$\dot{x} = v\cos\theta \tag{3.1}$$

$$\dot{y} = v\sin\theta \tag{3.2}$$

$$\dot{\theta} = \omega, \tag{3.3}$$

where the state is $\begin{bmatrix} x \\ y \\ \theta \end{bmatrix}$ and the input is $\begin{bmatrix} v \\ \omega \end{bmatrix}$. The next section examines the design of the lateral controller.

3.3 Design of the Lateral Controller

We have used the path tracker described in Marshall et al. (2008). This pathtracking controller is a nonlinear controller that uses full-state feedback linearization. We make the following assumptions about this controller:

1. The linear speed of the follower is constant.

2. The follower's kinematics can be appropriately described by a unicycle model.

3. The reference path is a sequence of straight line segments.

Under these assumptions, we now examine the representation of the leader's path and the definitions of the error terms.

3.3.1 Path Representation and Error Terms

All the signals are at time $t \geq 0$ unless otherwise stated.

A convoy of autonomous followers with a manually-driven leader can be made to traverse a 2D terrain in the following different scenarios:

1. The convoy of vehicles travels a path in an outdoor environment using the VT&R method. Here, the leader uses a visual sensor to build a map of 3D landmarks with respect to the reference frame attached to it.

2. The convoy of vehicles traverses a path in the Vicon lab, which is an indoor test facility. Here, the Vicon cameras can be used for measuring the poses of the vehicles

in the Vicon frame. So, as the leader travels, its position and headings defined in the Vicon frame can be obtained at different time steps by communicating with the Vicon system over a WiFi network. Thus, the leader's path is defined by an array of poses and can be stored in a computer's file.

3. A simulation model is designed for the scenario when the convoy of vehicles moves in the Vicon lab. Simulations are performed in MATLAB, where the manually-driven leader is simulated by specifying a speed and angular velocity. The leader's position and heading at different time steps can be obtained by the discretizing the differential equations described by (3.1)-(3.3).

In this chapter, we are considering the third case. For this case, the leader's path can be defined for the following two different situations:

1. The leader performs the teach pass and completes a path traversal. The entire path is stored with respect to the Vicon frame. Then the followers repeat the leader's path after a long time, maybe the next day, with no leader physically present at the time of execution. So, if the leader travels for a time duration t_f, then a set of poses, $P_0 = \{x_0(\tau), y_0(\tau), \theta_0(\tau) : 0 \leq \tau \leq t_f\}$, is obtained. Here, the teach pass and the repeat pass do not occur simultaneously.

2. The leader and the followers travel together and the leader's path is defined only till the current time t. This refers to the convoying problem. In this case, the teach pass and the repeat pass occur simultaneously, where the leader performs the route teaching and all the followers repeat the leader's path. Here, the set P_0 is defined as $P_0 = \{x_0(\tau), y_0(\tau), \theta_0(\tau) : 0 \leq \tau \leq t\}$. In this case, P_0 is a function of t.

For each of the above two cases, the follower saves the set P_0. Let (x_d, y_d, θ_d) denote the closest pose in P_0 to the follower's position (x, y), that is,

$$(x_d, y_d) = \underset{(x_0, y_0) \in P_0}{\arg\min} \|(x, y) - (x_0, y_0)\|$$

and θ_d is the heading angle associated with the position (x_d, y_d).

The error terms are defined as shown in Figure 3.4. Notice that the lateral error is calculated with respect to the reference path passing through (x_d, y_d) and having a slope, $\tan\theta_d$. After a reference path is obtained, the follower aims to follow the path and not the desired pose, that is, the problem is one of path following and not trajectory tracking. Thus, the position of the desired pose on the path is irrelevant to the follower. The lateral error, e_{L}, and the heading error, e_{H}, are computed according to

$$e_{\mathrm{L}} = -(x - x_d)\sin\theta_d + (y - y_d)\cos\theta_d \tag{3.4}$$

$$e_{\mathrm{H}} = \theta - \theta_d. \tag{3.5}$$

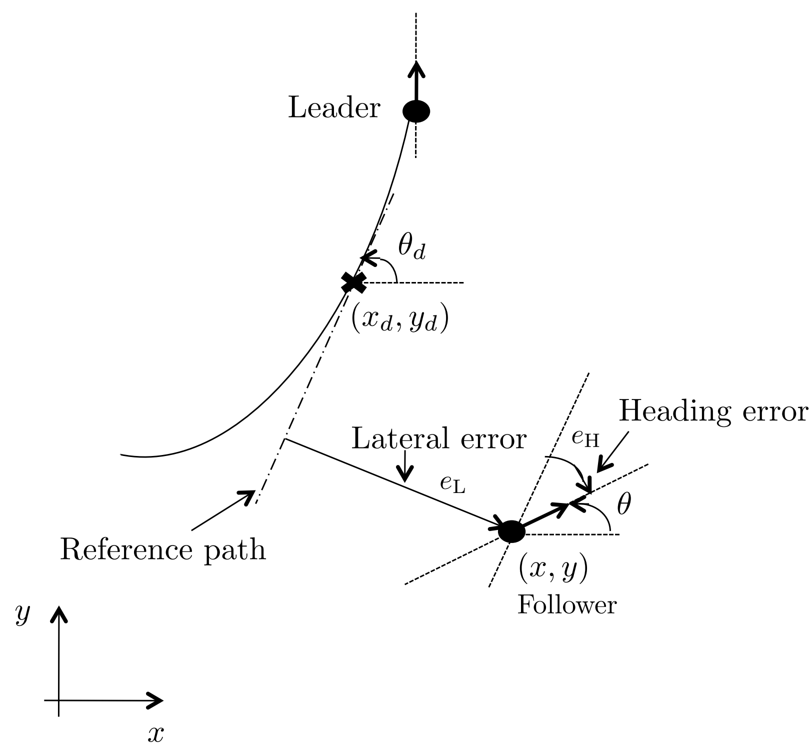

Figure 3.4: Error terms.

The next section describes the path-tracking controller designed to drive e_{L} and e_{H} to zero.

3.3.2 Design of the Rotational Control Input ω

The system of equations describing the lateral and heading error rates is obtained by differentiating (3.4) and (3.5). Thus,

$$\begin{aligned}
\dot{e}_{\mathrm{L}} &= -(\dot{x}-\dot{x}_d)\sin\theta_d + (\dot{y}-\dot{y}_d)\cos\theta_d - (y-y_d)(\sin\theta_d)\dot{\theta}_d - (x-x_d)(\cos\theta_d)\dot{\theta}_d \\
&= -\dot{x}\sin\theta_d + \dot{y}\cos\theta_d + \dot{x}_d\sin\theta_d - \dot{y}_d\cos\theta_d \\
&\quad - \big((x-x_d)\cos\theta_d + (y-y_d)\sin\theta_d\big)\dot{\theta}_d \qquad (3.6)\\
\dot{e}_{\mathrm{H}} &= \dot{\theta} - \dot{\theta}_d. \qquad (3.7)
\end{aligned}$$

As the position of the point (x_d, y_d) on the reference line is irrelevant for path tracking purposes, therefore the term $\big((x-x_d)\cos\theta_d + (y-y_d)\sin\theta_d\big)$ can be neglected. Also,

$$\dot{x}_d\sin\theta_d = \dot{y}_d\cos\theta_d. \qquad \text{from (3.1) and (3.2)} \qquad (3.8)$$

Therefore

$$\begin{aligned}
\dot{e}_{\mathrm{L}} &= -\dot{x}\sin\theta_d + \dot{y}\cos\theta_d \\
&= -v\cos\theta\sin\theta_d + v\sin\theta\cos\theta_d \qquad \text{from (3.1) and (3.2)} \\
&= v\sin(\theta-\theta_d) \\
&= v\sin e_{\mathrm{H}}. \qquad \text{from (3.5)} \qquad (3.9)
\end{aligned}$$

If the leader's steering angle changes by a small quantity as compared to follower's steering angle changes, then $\dot{\theta}_d$ can be neglected in (3.7). Under this assumption the heading error dynamics is

$$\dot{e}_{\mathrm{H}} = \dot{\theta} = \omega. \quad \text{from (3.3)} \qquad (3.10)$$

Hence, the equations describing the error dynamics are

$$\begin{bmatrix} \dot{e}_{\mathrm{L}} \\ \dot{e}_{\mathrm{H}} \end{bmatrix} = \begin{bmatrix} v\sin e_{\mathrm{H}} \\ \omega \end{bmatrix}. \qquad (3.11)$$

A substitution of variables is used to transform the above nonlinear system into a linear system. Let $z_1 := e_{\mathrm{L}}$ and $z_2 := v \sin e_{\mathrm{H}}$. The new system of equations is given by

$$\begin{bmatrix} \dot{z}_1 \\ \dot{z}_2 \end{bmatrix} = \begin{bmatrix} 0 & 1 \\ 0 & 0 \end{bmatrix} \begin{bmatrix} z_1 \\ z_2 \end{bmatrix} + \begin{bmatrix} 0 \\ v\omega \cos e_{\mathrm{H}} \end{bmatrix} = \begin{bmatrix} 0 & 1 \\ 0 & 0 \end{bmatrix} \begin{bmatrix} z_1 \\ z_2 \end{bmatrix} + \begin{bmatrix} 0 \\ \eta \end{bmatrix}, \tag{3.12}$$

where the new control input in these transformed coordinates is defined as

$$\eta := v\omega \cos e_{\mathrm{H}}. \tag{3.13}$$

Choosing a proportional controller of the form

$$\eta = -k_{L1} z_1 - k_{L2} z_2 \tag{3.14}$$

gives the following closed-loop error dynamics:

$$\dot{z} = \begin{bmatrix} 0 & 1 \\ -k_{L1} & -k_{L2} \end{bmatrix} z. \tag{3.15}$$

As long as $k_{L1}, k_{L2} > 0$, this system will be stable.

Using (3.13) and (3.14), the control input, ω, is given by

$$\omega = \frac{-k_{L1} z_1 - k_{L2} z_2}{v \cos e_{\mathrm{H}}}.$$

On back substituting the values of z_1 and z_2 we get

$$\omega = \frac{-k_{L1} e_{\mathrm{L}} - k_{L2} v \sin e_{\mathrm{H}}}{v \cos e_{\mathrm{H}}}. \tag{3.16}$$

In order to get a finite value of ω, the denominator of (3.16) should not be zero. Thus, it must be ensured that neither v nor $\cos e_{\mathrm{H}}$ is zero.

3.3.3 Simulation Block Diagram of the Lateral Controller

For validation of the controller model, a simulation environment in MATLAB was created. The simulation block diagram of the leader and an autonomous follower is shown in

Figure 3.5. This diagram is similar to the block diagram shown in Figure 3.2 except that the leader model is included and the Vicon system is represented by corrupting the pose measurements. We have used the same follower's model to represent the leader. It should be noted that the block diagram shown in Figure 3.5 was discretized for performing simulations in MATLAB. This is in accordance with the Vicon system, which produces discrete-time outputs of the measured positions and headings of the vehicles. The speed, steering, and pose measurements are corrupted by zero mean white Gaussian noises. In practice, the noises may not necessarily be Gaussian. We chose Gaussian because our aim is not to accurately model the noises but to test the robustness of our design. It should be noted that for calculating the nearest pose point in P_0 to the follower's current position, the entire set P_0 is not required to be searched by the follower. A search length, δ, can be specified from the last desired pose. Hence, when beginning a new search, the follower will disregard all the poses till the last desired pose and will only need δ successive points in P_0 from the last desired pose. This will lead to faster follower performance as the follower is not required to save the entire set P_0 as it moves.

In Figure 3.5, the only other parameter that needs to be determined is the speed input, v_i, to the follower. As the lateral controller is aimed to keep the follower on the leader's path in 2D, v_i can be chosen so that a desired spacing between the leader and the follower is maintained. Thus, calculating the desired speed, v_i, is a 1D spacing problem and the longitudinal controller described in Chapter 2 can be used. The next section examines the combined block diagram of the lateral controller in 2D and the longitudinal controller in 1D.

3.4 The Lateral and Longitudinal Controllers

In order to use the longitudinal controller described in Chapter 2, a $h(q)$ function needs to be specified. In 1D the variable q represents the distance from the starting point of

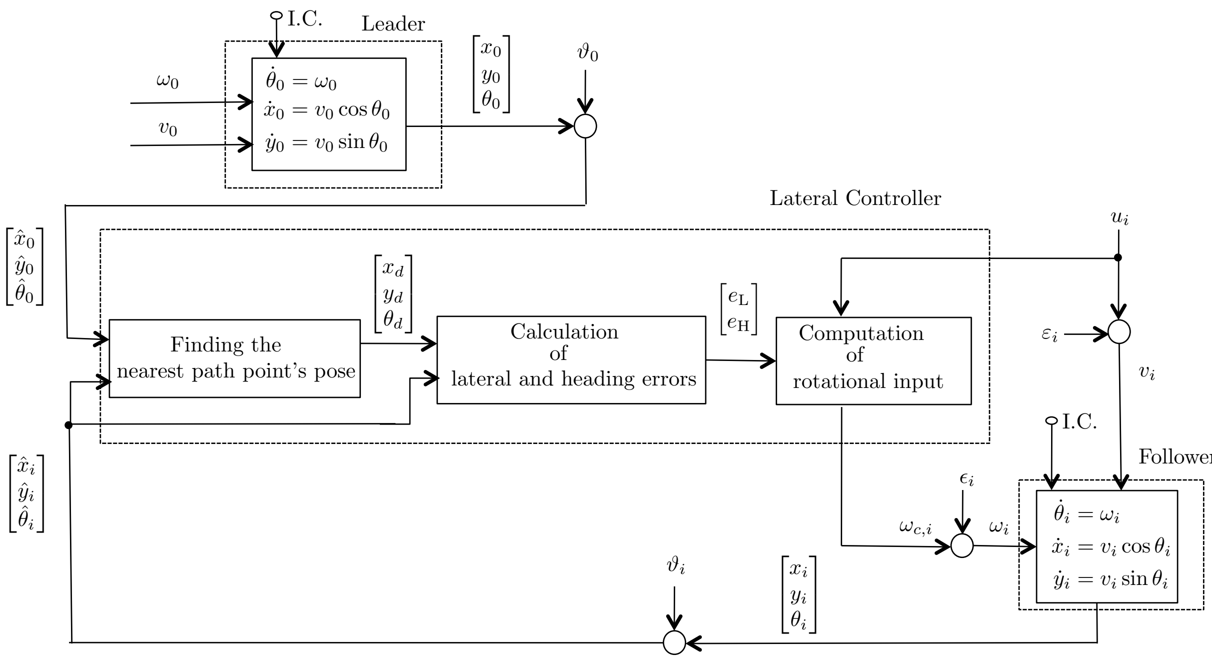

Figure 3.5: Simulation block diagram of the lateral controller with the leader and the i^{th} follower.

the convoy. Equivalently, in 2D the arc length of the path from the starting point of the convoy can be used to represent q. Accordingly, the $h(q)$ function is replaced by $h(p)$, where p is the arc length of the path from the starting point. The output of the $h(p)$ function is corrupted by zero mean white Gaussian noises to account for the noise present in the pose measurements. Figure 3.6 shows the combined block diagram of the lateral and longitudinal controllers.

3.4.1 System Parameters

For the lateral controller, the closed loop characteristic polynomial of (3.15) is given as

$$s^2 + k_{L2}s + k_{L1}, \tag{3.17}$$

which represents a second-order system. We set the desired characteristic polynomial to

$$s^2 + 2\zeta\omega_n s + \omega_n^2, \tag{3.18}$$

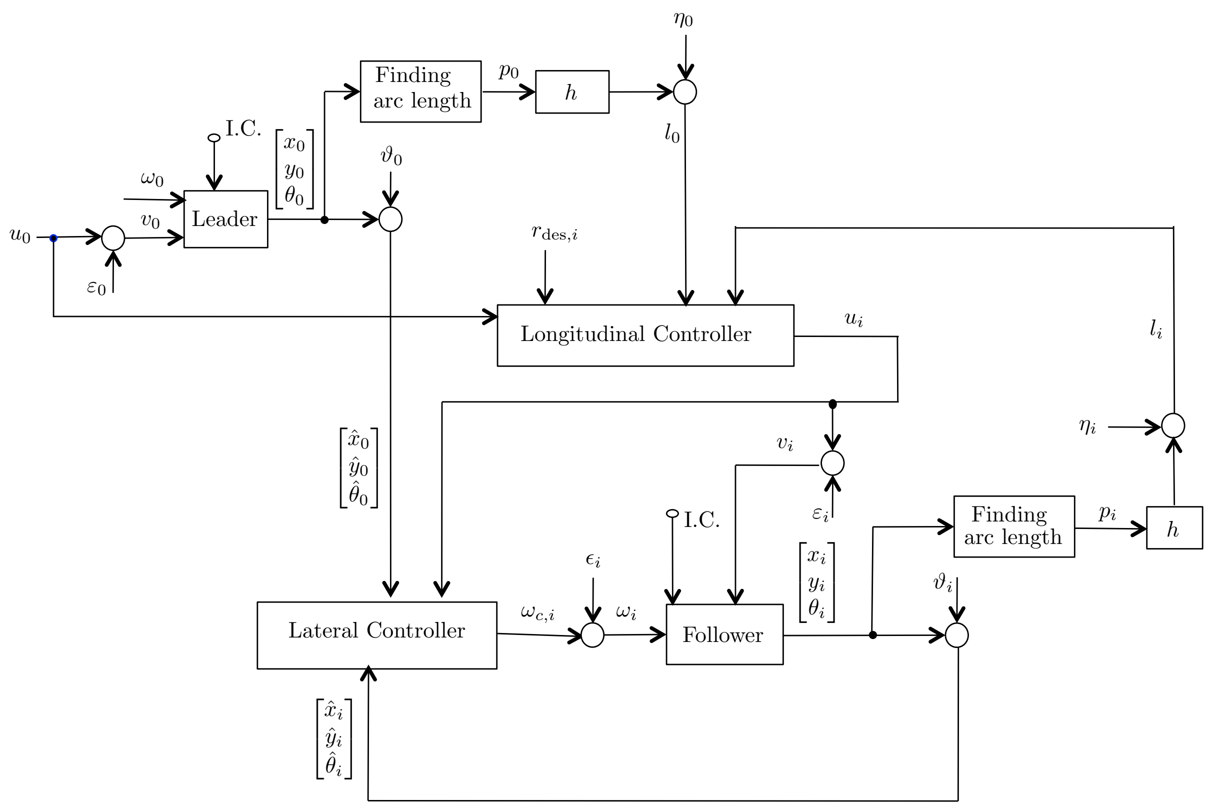

Figure 3.6: Simulation block diagram of the lateral and longitudinal controllers with the leader and the i^{th} follower.

where ζ is the damping ratio and ω_n is the natural frequency. On comparing (3.17) and (3.18), we get the design parameters as $k_{L1} = \omega_n^2$ and $k_{L2} = 2\zeta\omega_n$. The damping ratio and the natural frequency can be calculated from the percent overshoot $\%O.S.$, and the settling time T_s:

$$\zeta = \frac{-\ln \frac{\%O.S.}{100}}{\sqrt{\pi^2 + \ln^2 \frac{\%O.S.}{100}}} \tag{3.19}$$

and

$$\omega_n = \frac{-\ln(0.02\sqrt{1-\zeta^2})}{\zeta T_s}. \tag{3.20}$$

The desired $\%O.S.$ is set to 4.3% and T_s is taken as 10 s. Accordingly, $\zeta = 0.707$ and $\omega_n = 0.602$. Thus, $k_{L1} = 0.363$ and $k_{L2} = 0.852$.

For the longitudinal controller, the desired τ is taken to be 10 s. The $h(p_i)$ function is $0.5p_i$. Accordingly, the longitudinal gain is $k_1 = 0.2$. Table 3.1 summarizes the parameters used in the model along with their simulation values.

Description	Symbol	Value
Measured speed of the leader	u_0	0.1 m/s
Process noise variance on speed	σ_u^2	4×10^{-8} m^2/s^2
Process noise variance on pose	σ_ϑ^2	4×10^{-8}
Process noise variance on angular velocity	σ_ϵ^2	4×10^{-8} rad^2/s^2
Desired inter-vehicle distance	$r_{\text{des},i}$	1 m
$h(p_i)$ function	h	$0.5p_i$
Process noise variance on the measurement of h	σ_h^2	4×10^{-4} m^2
Longitudinal error gain	k_i	0.2
Lateral error gains	k_{L1} and k_{L2}	0.363 and 0.852

Table 3.1: Parameters used in the simulation model with both lateral and longitudinal controllers. The process noises are implemented as discrete-time signals in MATLAB.

Simulations were performed for the block diagram shown in Figure 3.6 with one and six followers to validate the controller design. The manually-driven leader was simulated by defining a constant speed of 0.1 m/s and a waveform for ω_0 as shown in Figure 3.7. The Vicon system outputs the heading angles between $-\pi$ to π. Accordingly, the heading angles were wrapped between $-\pi$ to π during the simulations, too. The dimension of the Vicon lab is approximately 23 m $\times$ 8 m. This dimension was taken into consideration while defining the leader's path. Figure 3.8 shows the leader's path defined in the Vicon lab. For realizing the situations when the leader is not in the line of sight of the followers, obstacles are placed in the lab as shown in Figure 3.8. The search length, δ, is set to 30 points. The initial positions of the vehicles are (14, -4). The longitudinal errors when the followers start are 0 m. The next section presents the simulation results.

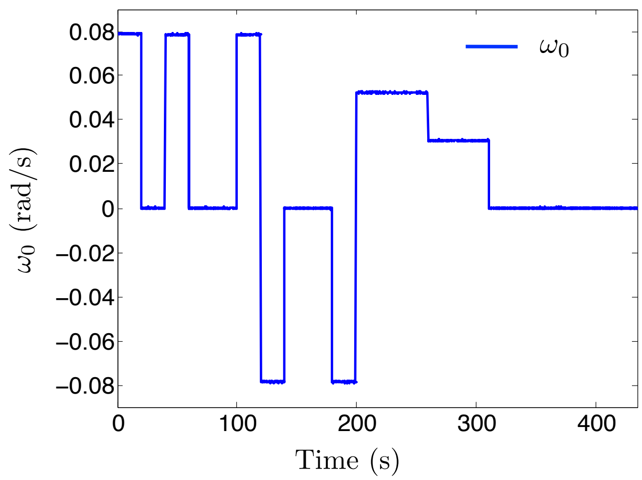

Figure 3.7: Specified angular velocity of the leader for simulations.

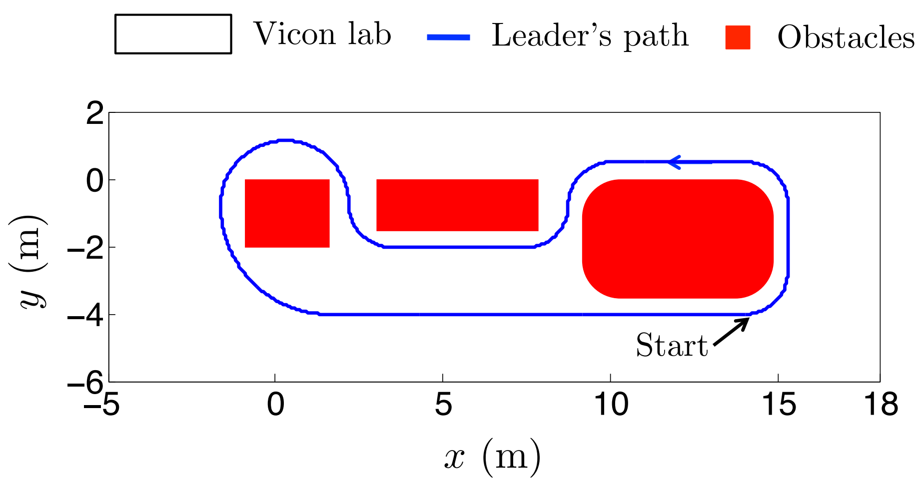

Figure 3.8: Leader's path defined in the Vicon lab along with obstructions.

3.4.2 Simulation Results

One follower

Figure 3.9 and Figure 3.10 show the simulation results with one follower. Figure 3.9a shows the paths of the leader and the follower. The close-up of the two paths is shown in

Figure 3.9b, where a lateral error between the two paths can be seen. The $h(p)$ function plot is shown in Figure 3.10a. Figure 3.10b and Figure 3.10c show the lateral and heading errors of the follower. As the heading angles of the vehicles are defined in the interval $[-\pi, \pi]$, jumps can be seen in the lateral and heading errors when the follower is taking a turn. The lateral error goes to zero for straightaways but not for turns as seen in Figure 3.9b. This is because the design of the lateral controller makes the assumption that the reference path is a sequence of straight line segments. The maximum lateral error is 0.021 m and the maximum heading error is 0.126 rad. The longitudinal error is shown in Figure 3.10d.

Six Followers

In this case, simulations were performed for the following two different cases to examine the performance of the controller design: (Sa) when all the followers were referencing the leader for calculating the error terms. This is referred as the absolute case. (Sb) when each follower is referencing the vehicle in front of it for calculating the error terms. This is called the relative case. In each case, the rms values of all the error terms were calculated for all the followers.

Simulation results for (Sa) are shown in Figure 3.11. As can be seen in Figure 3.11b, the deviation from the leader's path is almost the same for all the followers as each of the followers is referencing the leader for calculating the error terms. Therefore, the error in tracking the leader's path by the $(i-1)^{\text{th}}$ follower is not affecting the tracking performance of the i^{th} follower. However, the simulation result for (Sb) shown in Figure 3.12b implies that the deviation from the leader's path is increasing as the number of followers is increasing, that is, the error is accumulating. This behavior is observed as the i^{th} follower is referencing the $(i-1)^{\text{th}}$ follower and not the leader. So, the error values seen by the $(i-1)^{\text{th}}$ follower are inherently passed on to the i^{th} follower. As a result, the errors will keep on increasing as the number of vehicles increases and the tracking

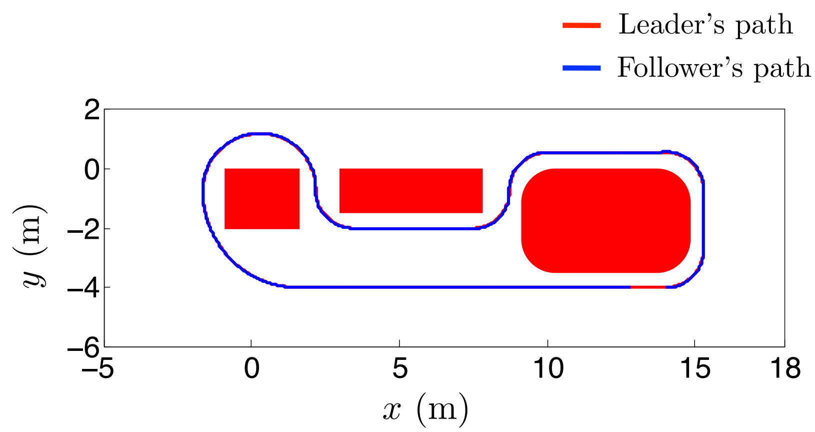

(a)

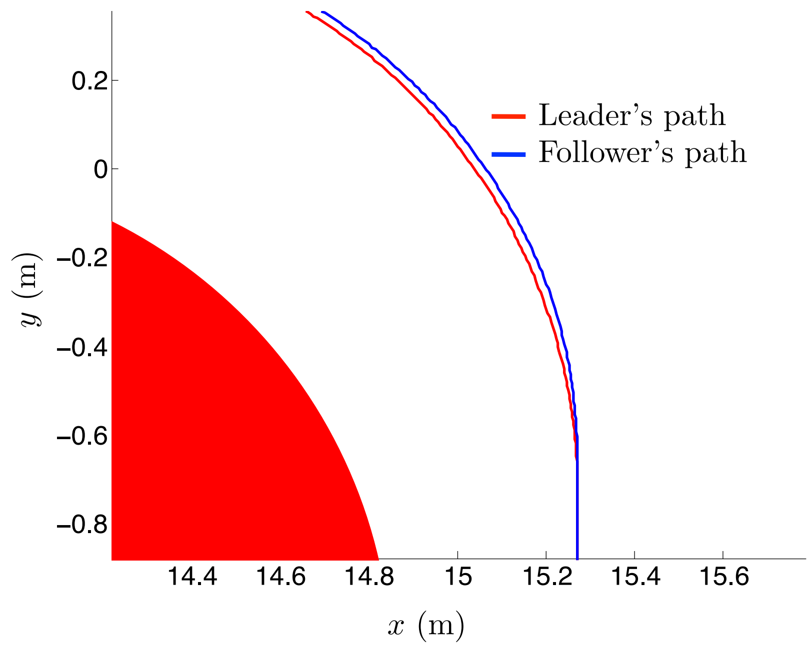

(b)

Figure 3.9: Simulated plots for one follower: (a) Leader's and follower's paths. (b) Close-up of the paths.

performance will not be robust to follower number. It should be noted that the scales of the plots for Figure 3.11b and Figure 3.12b are very different.

Figure 3.13 shows the rms value of errors of the followers for the absolute and relative cases. As zero-mean white Gaussian noises are added to the model, slight variations in the rms value of the errors can be seen even for the first follower in the absolute and relative case. It can be observed that the performance of the followers keeps on degrading in the relative case.

We conclude that the controller design works satisfactorily for the absolute case and the errors do not grow unbounded on adding more follower vehicles.

3.5 Self-intersecting Path

So far, simulation results are shown for a closed path that does not intersect itself at any point. In order to gauge the performance of the controller for the case when the path is self-intersecting, simulations were performed for the block diagram shown in Figure 3.6 with two followers. The absolute case as discussed in (Sa) is considered for calculating the error terms. The manually-driven leader was simulated by defining a constant speed of 0.1 m/s and a waveform for ω_0 as shown in Figure 3.14a. Figure 3.14b shows the leader's path in the Vicon lab. The initial positions of the vehicles are (0, 0). The search length, δ, is again taken to be 30 points. The longitudinal errors when both the followers start are 0 m. All other parameters are taken as defined in Table 3.1. Figure 3.14c shows the path of the vehicles and a close-up of the intersecting points is shown in Figure 3.14d. Each of the followers tracks the leader's path even when it re-visits a previous point on the path with a desired spacing of 1 m as seen in Figure 3.14c. Thus, the designed controller works well for a self-intersecting path too. However, the designed no collision algorithm does not take into consideration the collision that might occur at the intersecting point, if two or more vehicles are crossing the intersecting point at the same time.

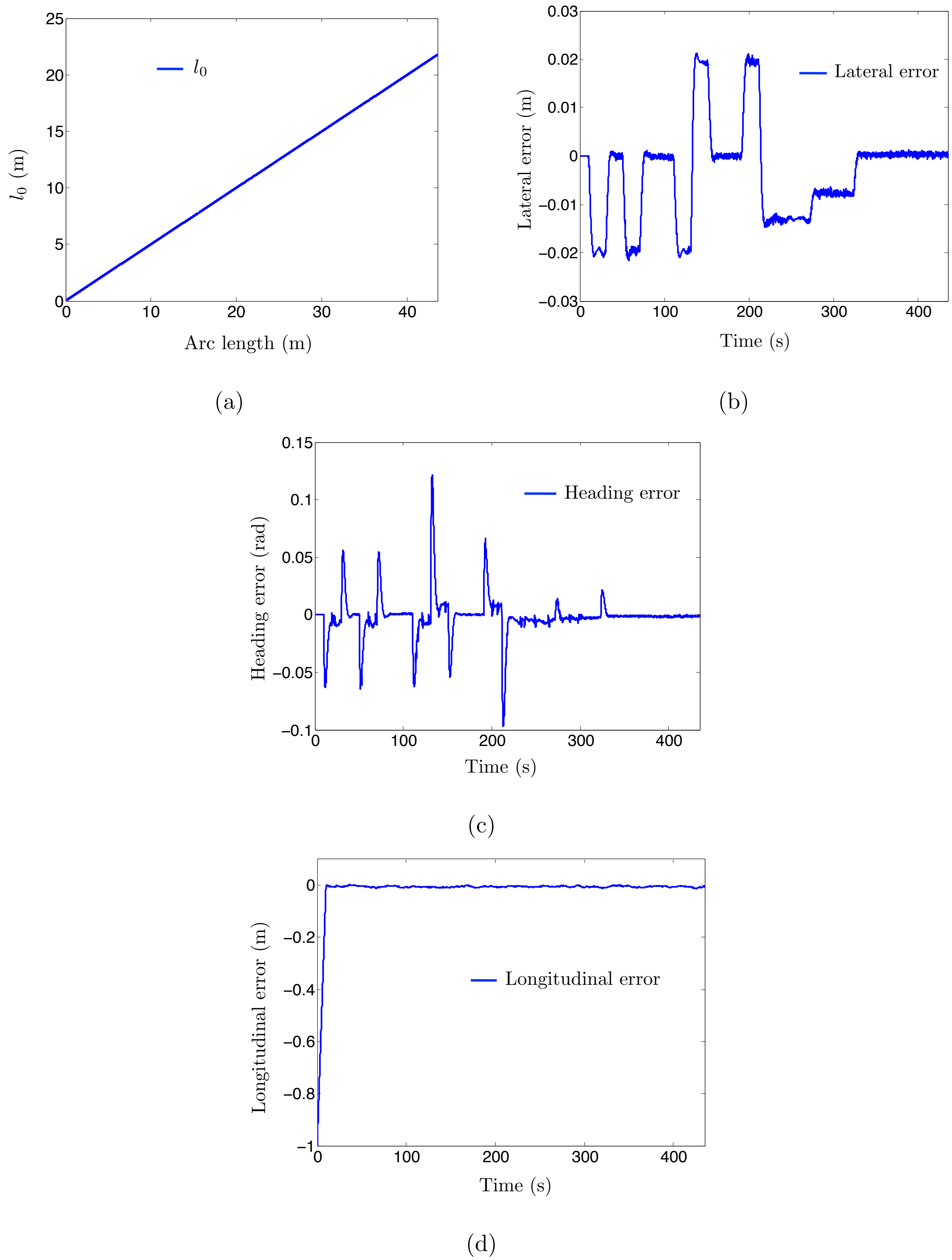

Figure 3.10: Simulated plots for one follower: (a) l_0 as measured by the leader. (b) The lateral error. (c) The heading error. (d) The longitudinal error.

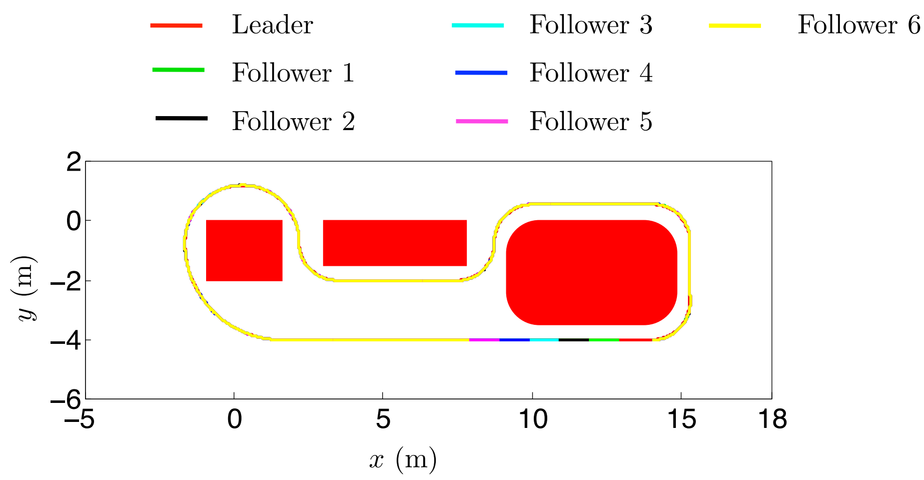

(a)

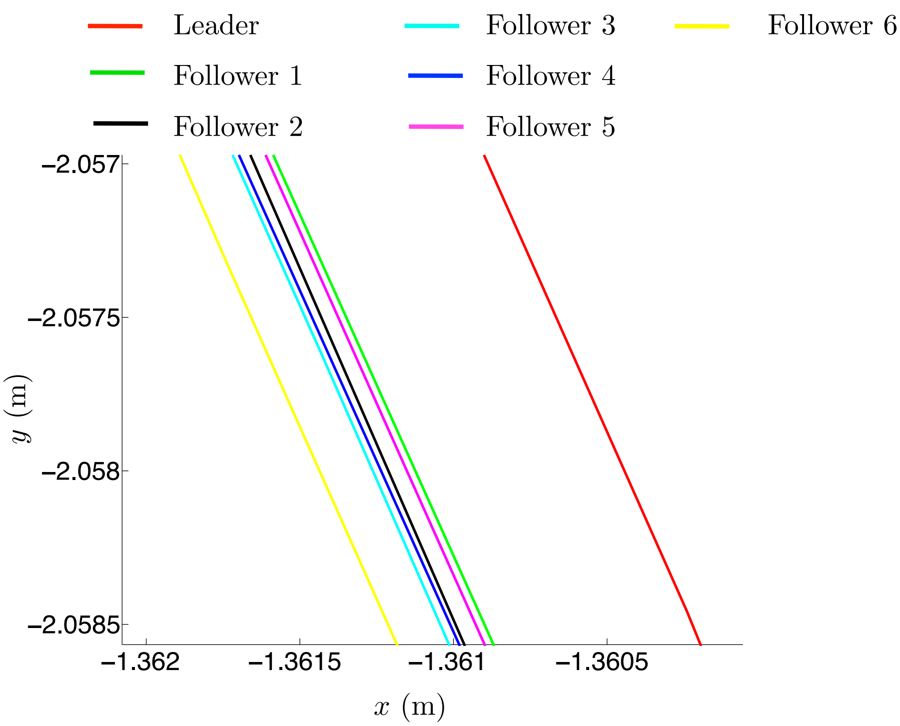

(b)

Figure 3.11: Simulated plots of six followers for the absolute case: (a) Leader's and follower's paths. (b) Close-up of the paths.

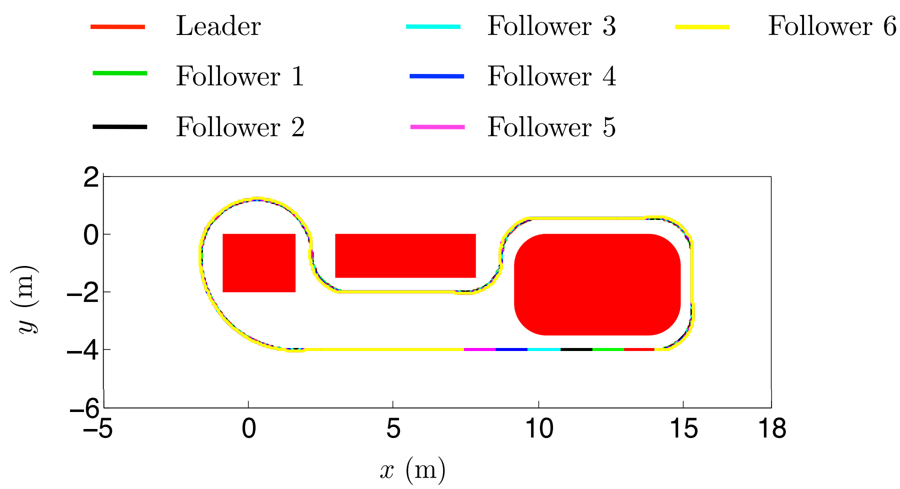

(a)

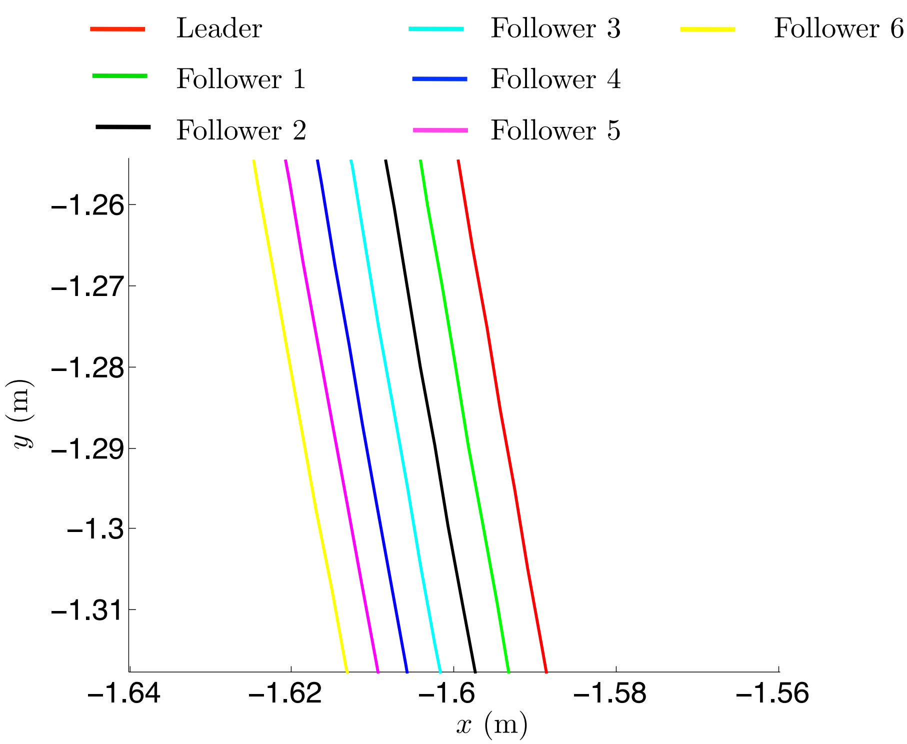

(b)

Figure 3.12: Simulated plots of six followers for the relative case: (a) Leader's and follower's paths. (b) Close-up of the paths.

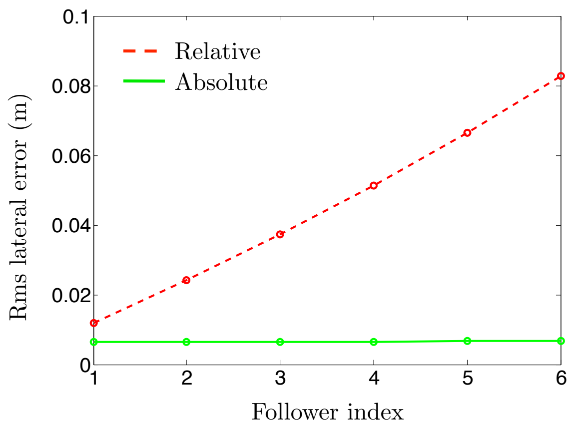

(a)

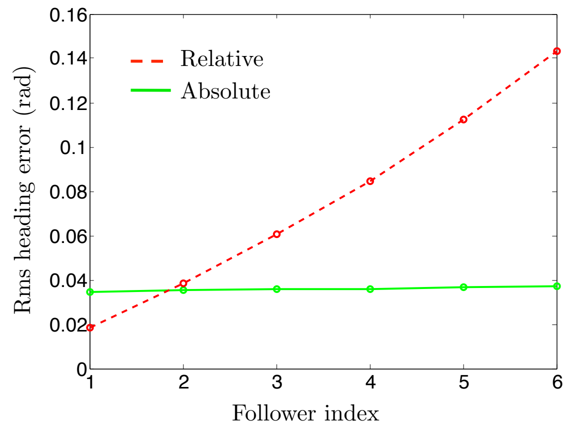

(b)

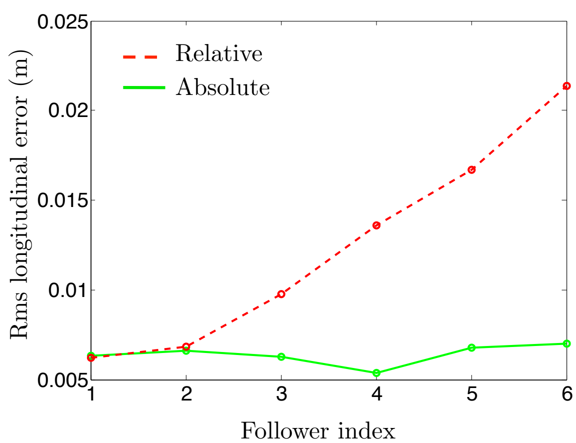

(c)

Figure 3.13: The rms value of errors for the relative and absolute case: (a) The lateral error. (b) The heading error. (c) The longitudinal error.

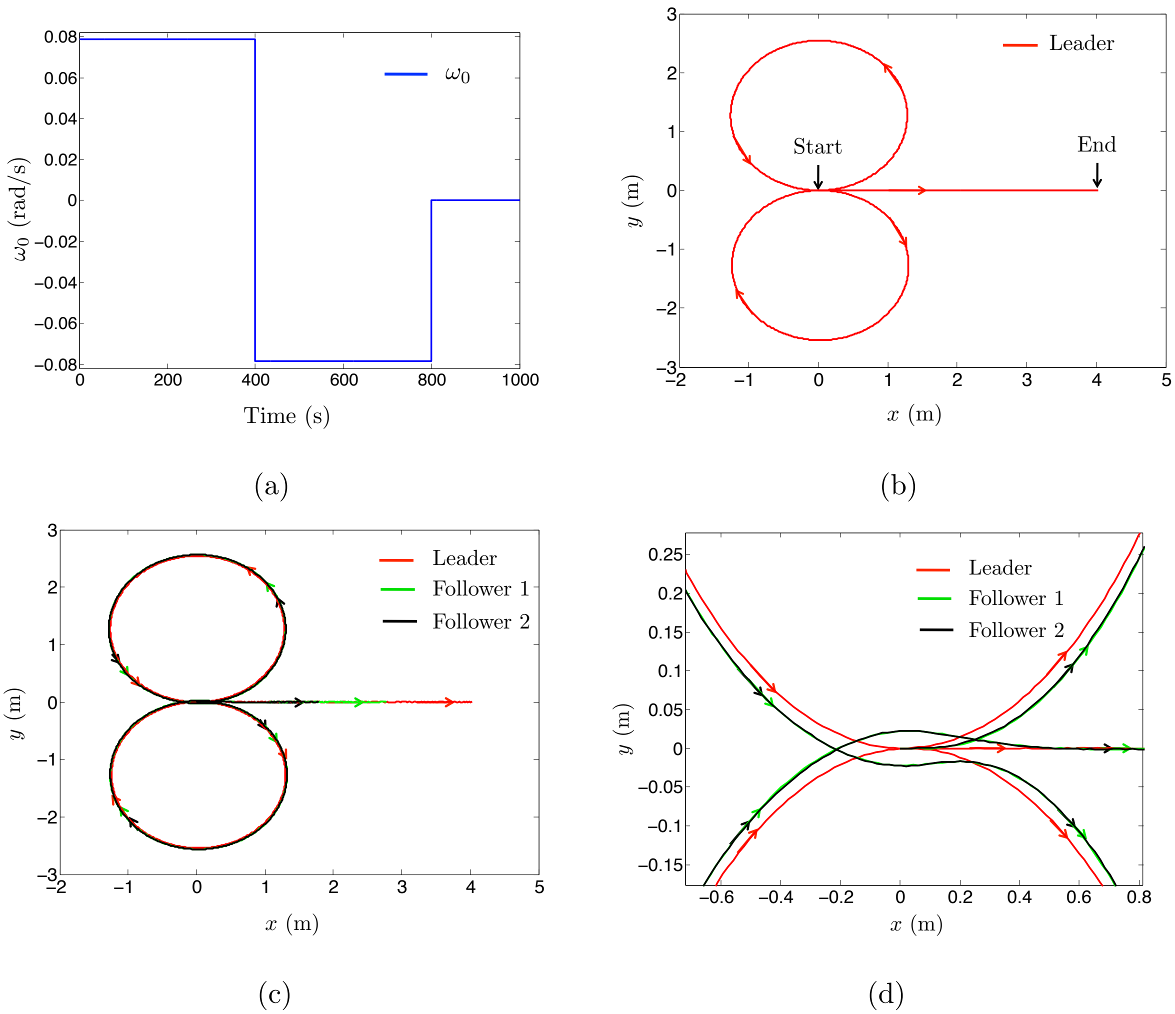

Figure 3.14: Simulated plots for a self-intersecting path: (a) Specified angular velocity of the leader. (b) Leader's path in the Vicon lab. (c) Leader's and follower's paths. (d) Close-up of the intersecting points.

Chapter 4

Conclusions and Future Work

This thesis provides a detailed design and simulation validation of a distributed control law that uses the idea behind the VT&R method to allow a convoy of inter-communicable autonomous vehicles to follow a manually-driven lead vehicle's path with a desired inter-vehicle spacing, even when the leader is not in the camera view of the followers. The use of GPS, lane markers/magnets, and/or a vision-based convoying is avoided and the vehicles are equipped with wheel encoders and a monocular camera, and have computational capability.

In the design of the longitudinal controller in 1D, a very idealized situation is considered where the vehicles are modeled as kinematic integrators. For incorporating the concept of VT&R, further simplification is made by assuming that there is a hill that can be seen by all the vehicles and the hill's profile is captured by a monotonically increasing linear function of the distance travelled by the vehicles. The elevation of the hill is measured by the camera to be used as landmarks for map building. The vehicle dynamics is treated as unity gain and the controller is designed based solely on the vehicle kinematics. The longitudinal controller is designed by assuming that the hill's profile is successfully captured by a monotonically increasing linear function. Simulations were performed in MATLAB for a variety of operating conditions with one and two followers. Noises in sensor measurements are also modeled as zero-mean white Gaussian noises.

For addressing the convoy problem in 2D, the designed longitudinal controller in 1D is combined with a path tracker. The path tracker helps the follower vehicles to successfully track the leader's path while the longitudinal controller controls the inter-vehicle spacing. The goal is to use the Vicon system for inter-communicating the vehicles poses. The map building for the longitudinal controller is based on the arc length of the path travelled. For the path tracker, the unicycle model is used to model the vehicle kinematics. Simulations were performed in MATLAB with one and six followers to validate the controller design. With six followers, simulation results are shown for the following two different cases: (1) when all the followers are referencing the leader for calculating the error terms and (2) when each follower is referencing the vehicle in front of it for calculating the error terms. Results obtained show that the controller design works satisfactorily for the first case and the errors do not grow unbounded on adding more follower vehicles. The designed controller also works well for self-intersecting paths.

However, experimental trials were not performed in the Vicon lab because of lack of time. It is hoped that the controller design presented in this thesis would be eventually incorporated in convoying based on VT&R.

4.1 Future Work

The presented control design serves as a starting point to incorporate VT&R for the longitudinal control in a convoy problem. A number of simplifications were made to achieve a working model. This section briefly discuss the areas of future work and improvements that can be made.

Improvements in the controller design

The longitudinal controller is designed for a very idealized situation. It does not take into account the dynamics present in the vehicle model and VT&R concept is incorporated by using a linear function to build a map. These simplifications need to be modified by a more robust design model. For a self-intersecting path, the no collision algorithm needs to be modified too.

Extension to the real world

The simulation model presented in this thesis is designed for a Vicon lab, which provides an indoor test facility. Experimental trials are needed to validate the simulation model for the Vicon lab. After this, future work should consider using the proposed method for a real-time VT&R convoying.

Appendix A

Derivation of the Unicycle Model

Consider a point moving in a plane as shown in Figure A.1. The state variables are the

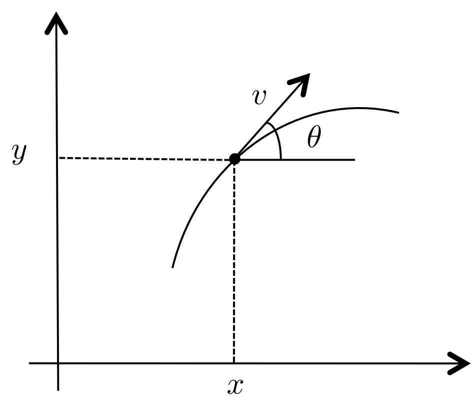

Figure A.1: Unicycle model kinematics.

coordinates of the point, (x, y), and the heading angle, θ. The forward velocity of the moving point is v. In $\mathbb{C}$, the position of the point is defined as

$$z := x + jy.$$

Thus, the velocity is

$$\dot{z} = \dot{x} + j\dot{y}. \tag{A.1}$$

In polar form, the velocity is defined as $v\mathrm{e}^{j\theta}$, where $v \geq 0$. So, by identifying $\dot{z}$ and $ve^{j\theta}$ we get

$$v\mathrm{e}^{j\theta} = \dot{x} + j\dot{y}. \tag{A.2}$$

Recall Euler's formula:

$$\mathrm{e}^{j\theta} = \cos\theta + j\sin\theta.$$

Substitute into (A.1) to get

$$v(\cos\theta + j\sin\theta) = \dot{x} + j\dot{y}.$$

On comparing the real and imaginary parts of the above equation, we have

$$\dot{x} = v\cos\theta$$
$$\dot{y} = v\sin\theta.$$

Finally, the angular velocity, ω, is defined as

$$\omega = \dot{\theta}.$$

Thus, the kinematic model equations of the unicycle are

$$\dot{x} = v\cos\theta \tag{A.3}$$
$$\dot{y} = v\sin\theta \tag{A.4}$$
$$\dot{\theta} = \omega. \tag{A.5}$$

Appendix B

Derivation of the Error Terms

For understanding the definitions of the error terms, it is now convenient to turn to the complex plane. In $\mathbb{C}$, let the desired pose be $z_d = x_d + jy_d$ with a heading vector $e^{j\theta_d}$. Likewise, the follower's pose is $z = x + jy$ and its heading vector is $e^{j\theta}$ as shown in Figure B.1a. Thus, the point, z_d, and the heading vector, $e^{j\theta_d}$, define a coordinate frame Σ_d. The error vector is defined to be the vector $z - z_d$ in the frame Σ_d as shown in Figure B.1b. For defining the lateral error term, the definition of the dot product of two vectors in $\mathbb{C}$ is presented next.

B.1 Representation of dot product in $\mathbb{C}$

For vectors $A = [a_1 \quad a_2]^T$ and $B = [b_1 \quad b_2]^T$, the dot product, $< A, B >$, in $\mathbb{R}^2$ is defined as

$$\begin{aligned} < A, B > &= A^T B \\ &= a_1 b_1 + a_2 b_2. \end{aligned}$$

In $\mathbb{C}$, the above vectors are defined as $A = |A|e^{j\phi_1}$ and $B = |B|e^{j\phi_2}$. If the angle between them is $\phi = \phi_1 - \phi_2$, the dot product, $< A, B >$, is given as

$$< A, B > = |A||B| \cos(\phi)$$

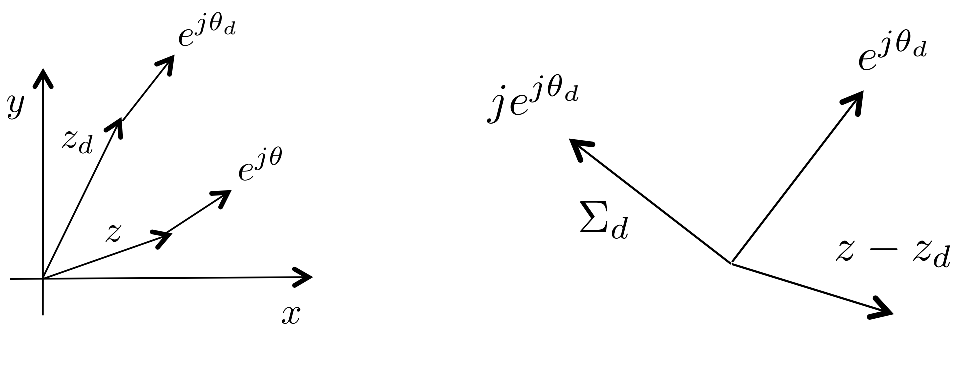

(a) (b)

Figure B.1: (a) Leader's and follower's positions and headings defined in the complex plane. (b) The error vector $z - z_d$ in the coordinate frame Σ_d.

$$
\begin{aligned}
&= |A||B|\cos(\phi_1 - \phi_2) \\
&= |A||B|(\cos\phi_1 \cos\phi_2 + \sin\phi_1 \sin\phi_2) \\
&= \sqrt{a_1^2 + a_2^2}\sqrt{b_1^2 + b_2^2}\left(\frac{a_1 b_1}{\sqrt{a_1^2 + a_2^2}\sqrt{b_1^2 + b_2^2}} + \frac{a_2 b_2}{\sqrt{a_1^2 + a_2^2}\sqrt{b_1^2 + b_2^2}}\right) \\
&= a_1 b_1 + a_2 b_2. \qquad (B.1)
\end{aligned}
$$

Also,

$$
\begin{aligned}
\bar{A}B &= (a_1 - ja_2)(b_1 + jb_2) \\
&= a_1 b_1 + a_2 b_2 + j(a_1 b_2 - a_2 b_1). \qquad (B.2)
\end{aligned}
$$

On comparing (B.1) and (B.2) we get

$$< A, B >= \Re(\bar{A}B).$$

Thus, from Figure B.1b the lateral error, e_{L}, is defined as $< z - z_d, je^{j\theta_d} >$, where

$$< z - z_d, je^{j\theta_d} >= \Re\big((\bar{z} - \bar{z}_d)je^{j\theta_d}\big).$$

Therefore

$$
\begin{aligned}
e_{\mathrm{L}} &= \Re\Big(\big((x-x_d)-j(y-y_d)\big)(j\cos\theta_d-\sin\theta_d)\Big) \\
&= \Re\big(-(x-x_d)\sin\theta_d+(y-y_d)\cos\theta_d+j\big((x-x_d)\cos\theta_d+(y-y_d)\sin\theta_d)\big) \\
&= -(x-x_d)\sin\theta_d+(y-y_d)\cos\theta_d. \qquad \text{(B.3)}
\end{aligned}
$$

The heading error is defined as

$$e_{\mathrm{H}} = \theta - \theta_d. \qquad \text{(B.4)}$$

Bibliography

H. Ando, Shiga, Y. Oasa, I. Suzuki, and M. Yamashita. Distributed memoryless point convergence algorithm for mobile robots with limited visibility. In *IEEE Transactions on Robotics and Automation,* volume 15(5), pp. 818-828, 1999.

H. Asama, A. Matsumoto, and Y. Ishida. Design of an autonomous and distributed robot system: ACTRESS. In *Proceedings of IEEE/RSJ International Workshop on Intelligent Robots and Systems,* pp. 283-290, 1989.

P. Avanzini, E. Royer, B. Thuilot, and P. Martinet. A global decentralized control strategy for urban vehicle platooning using monocular vision and a laser rangefinder. In *International Conference on Control, Automation, Robotics and Vision*, pp. 291-296, 2008.

P. Avanzini, B. Thuilot, T. Dallej, P. Martinet, and J.P. Derutin. On-line reference trajectory generation for manually convoying a platoon of automatic urban vehicles. In *IEEE/RSJ International Conference on Intelligent Robots and Systems*, pp. 1867-1872, 2009.

P. Avanzini, B. Thuilot, and P. Martinet. Accurate platoon control of urban vehicles, based solely on monocular vision. In *IEEE/RSJ International Conference on Intelligent Robots and Systems*, pp. 6077- 6082, 2010.

P. Avanzini, B. Thuilot, and P. Martinet. Manual convoying of automated urban vehicles relying on monocular vision. In *IEEE Intelligent Vehicles Symposium (IV)*, pp. 19-24, 2012.

T. Balch and R. C. Arkin. Communication in reactive multiagent robotics systems. In *Autonomous Robots,* volume 1(1), pp. 1-25, 1994.

S. Benhimane, E. Malis, P. Rives, and J. R. Azinheira. Vision-based control for car platooning using homography decomposition. In *IEEE International Conference on Robotics and Automation*, pp. 2161-2166, 2005.

J. Bom, B. Thuilot, F. Marmoiton, and P. Martinet. A global control strategy for urban vehicles platooning relying on nonlinear decoupling laws. In *IEEE/RSJ International Conference on Intelligent Robots and Systems*, pp. 2875-2880, 2005a.

J. Bom, B. Thuilot, F. Marmoiton, and P. Martinet. Nonlinear control for urban vehicles platooning, relying upon a unique kinematic GPS. In *Proceedings of the IEEE International Conference on Robotics and Automation*, pp. 4138-4143, 2005b.

J. Borenstein and Y. Koren. The vector field histogramfast obstacle avoidance for mobile robots. In *IEEE Journal of Robotics and Automation*, volume 7(3), pp. 278-288, 1991.

K. S. Chang, W. Li, P. Devlin, A. Shaikhbahai, P. Varaiya, J. K. Hedrick, D. McMahon, V. Narendran, D. Swaroop, and J. Olds. Experimentation with a vehicle platoon control system. In *Vehicle Navigation and Information Systems Conference*, pp. 1117-1124, 1991.

E. Chown, S. Kaplan, and D. Kortenkamp. Prototypes, location, and associative networks (plan): Towards a unified theory of cognitive mapping. In *Cognitive Science*, volume 19, pp. 1-51, 1995.

S. M. Das, Y. C. Hu., C. S. G. Lee, and Yung-Hsiang Lu. An efficient group communication protocol for mobile robots. In *Proceedings of the 2005 IEEE International Conference on Robotics and Automation, ICRA*, pp. 87-92, 2005.

P. Daviet and M. Parent. Platooning for Small Public Urban Vehicles. In *International Symposium on Experimental Robotics*, pp. 345-354, 1995.

P. Daviet and M. Parent. Longitudinal and lateral servoing of vehicles in a platoon. In *Proceedings of the IEEE Intelligent Vehicles Symposium*, pp. 41-46, 1996.

J. Deneubourg, S. Goss, G. Sandini, F. Ferrari, and P. Dario. Self-organizing collection and transport of objects in unpredictable environments. In *Japan-U. S. A. Symposium on Flexible Automation,* pp. 1093-1098, 1990.

H. Fritz. Longitudinal and lateral control of heavy duty trucks for automated vehicle following in mixed traffic: experimental results from the CHAUFFEUR project. In *Proceedings of the IEEE International Conference on Control Applications*, volume 2, pp. 1348-1352, 1999.

T. Fukuda and S. Nakagawa. A dynamically reconfigurable robotic system (concept of a system and optimal configurations). In *Proceedings of IECON*, pp. 588-595, 1987.

P. Furgale and T. Barfoot. Visual teach and repeat for long-range rover autonomy. In *Journal of Field Robotics, special issue on "Visual mapping and navigation outdoors"*, volume 27(5), pp. 534-560, 2010.

S. K. Gehrig and F. J. Stein. A trajectory-based approach for the lateral control of car following systems. In *IEEE International Conference on Systems, Man, and Cybernetics*, volume 4, pp. 3596-3601, 1998.

H. K. Goi. Distributed Control for Vision-Based Convoying. M.A.Sc. Thesis, University of Toronto, 2009.

H. K. Goi, J. L. Giesbrecht, T. D. Barfoot, and B. A. Francis. Vision-based autonomous convoying with constant time delay. In *Journal of Field Robotics*, volume 27(4), pp. 430-449, 2010.

I. Haskara, C. Hatipoğlu, and U. Ozguner. Combined decentralized longitudinal and lateral controller design for truck convoys. In *IEEE Conference on Intelligent Transportation System*, pp. 123-128, 1997.

J. K. Hedrick, D. McMahon, V. Narendran, and D. Swaroop. Longitudinal vehicle controller design for IVHS systems. In *American Control Conference*, pp. 3107-3112, 1991.

N. Kehtarnavaz, N. C. Griswold, and J. S. Lee. Visual control of an autonomous vehicle (BART)-The vehicle-following problem. In *IEEE Transactions on Vehicular Technology*, 40(3), pp. 654-662, 1991.

G. Klančar, D. Matko, and S. Blažic. A control strategy for platoons of differential drive wheeled mobile robot. In *Robotics and Autonomous Systems*, volume 59, pp. 57-64, 2011.

P. V. Kokotovic, H. K. Khalil, and J. O'Reilly. Singular perturbation methods in control: Analysis and design. Philadelphia: Society for Industrial and Applied Mathematics, 1999.

Z. Lin, M. Broucke, and B. Francis. Local control strategies for groups of mobile autonomous agents. In *Proceedings of 42nd IEEE Conference on Decision and Control*, volume 1, pp. 1006-1011, 2003.

G. Lu and M. Tomizuka. A laser scanning radar based autonomous lateral vehicle following control scheme for automated highways. In *Proceedings of the American Control Conference*, volume 1, pp. 30-35, 2003.

M. Manz, T. Luettel, F. V. Hundelshausen, and H. Wuensche. Monocular model-based 3D vehicle tracking for autonomous vehicles in unstructured environment. In *IEEE International Conference on Robotics and Automation*, pp. 2465-2471, 2011.

D. A. Márquez-Gámez and M. Devy. Visual navigation of communicating vehicles in unknown and changing environment. In *IEEE International Conference on Electronics, Circuits and Systems (ICECS)*, pp. 673-676, 2011.

J. Marshall, T. D. Barfoot, and J. Larsson. Autonomous underground tramming for center-articulated vehicles. In *Journal of Field Robotics*, volume 25(6-7), pp. 400-421, 2008.

J. A. Marshall, M. E. Broucke, and B. A. Francis. Formations of vehicles in cyclic pursuit. In *IEEE Transactions on Automatic Control*, pp. 1963-1974, 2004.

M. Mataric. Interaction and Intelligent Behavior. Phd thesis, Massachsetts Institute of Technology, 1994.

D. McFarland. Towards robot cooperation. In *Proceedings of the Third International Conference on Simulation of Adaptive Behavior*, pp. 440-444, MIT press, 1994.

D. H. McMahon, V. K. Narendran, D. Swaroop, J. K. Hedrick, K. S. Chang, and P. E. Devlin. Longitudinal vehicle controllers for IVHS: Theory and Experiment. In *American Control Conference*, pp. 1753-1757, 1992.

C. McManus, P. Furgale, B. Stenning, and T. D. Barfoot. Visual teach and repeat using appearance-based lidar. In *IEEE International Conference on Robotics and Automation*, pp. 389-396, 2012.

P. Molnar and J. Starke. Communication fault tolerence in distributed robotic systems. In *Proceedings of Fifth International Symopsium on Distributed Autonomous Robotic Systems, (DARS)*, 2000.

K. C. Ng and M. M. Trivedi. Multirobot convoying using neuro-fuzzy control. In *Proceedings of the 13th International Conference on Pattern Recognition*, volume 4, pp. 417-421, 1996.

K. Ozaki, H. Asama, Y. Ishida, A. Matsumoto, K. Yokota, H. Kaetsu, and I. Endo. Synchronized motion by multiple mobile robots using communication. In *Proceedings of the 1993 IEEE/RSJ Intemational Conference on Intelligent Robots and Systems*, volume 2, pp. 1164-1169, 1993.

I. Papadimitriou, G. Lu, and M. Tomizuka. Autonomous lateral following considerations for vehicle platoons. In *Proceedings of the IEEE/ASME International Conference on Advanced Intelligent Mechatronics*, volume 1, pp. 401-406, 2003.

S. Premvuti and S. Yukta. Consideration on the cooperation of multiple autonomous mobile robots. In *Proceedings of the IEEE International Workshop of Intelligent Robots and Systems*, pp. 59-63, 1990.

H. Schneiderman, M. Nashman, A. J. Wavering, and R. Lumia. Vision-based robotic convoy driving. In *Machine Vision and Applications*, volume 8(6), pp. 359-364, 1995.

G. Sibley, C. Mei, I. Reid, and P. Newman. Vast-scale outdoor navigation using adaptive relative bundle adjustment. In *The International Journal of Robotics Research*, volume 29(8), pp. 958-980, 2010.

S. Simhon and G. Dudek. A global topological map formed by local metric maps. In *Proceedings of the IEEE/RSJ International Conference on Intelligent Robots and Systems*, volume 3, pp. 1708-1714, 1998.

A. Sinha and D. Ghose. Generalization of linear cyclic pursuit with application to rendezvous of multiple autonomous agents. In *IEEE Transactions on Automatic Control*, volume 51(11), pp. 1819-1824, 2006.

R. Sukthankar. RACCOON: A Real-time Autonomous Car Chaser Operating Optimally at Night. In *Proceedings of the IEEE Intelligent Vehicles Symposium*, pp. 37-42, 1993.

D. Swaroop and J. K. Hedrick. String stability of interconnected systems. In *IEEE Transactions on Automatic Control*, volume 41(3), pp. 349-357, 1996.

D. Swaroop, J. K. Hedrick, and S. B. Choi. Direct adaptive longitudinal control of vehicle platoons. In *IEEE Transactions on Vehicular Technology*, volume 50(1), 2001.

H. Tan, R. Rajamani, and W. Zhang. Demonstration of an automated highway platoon system. In *Proceedings of the American Control Conference*, volume 3, pp. 1823-1827, 1998.

W. Travis and D. M. Bevly. Trajectory duplication using relative position information for automated ground vehicle convoys. In *IEEE/ION Position, Location and Navigation Symposium*, pp. 1022-1032, 2008.

L. Vasseur, O. Lecointe, J. Dento, N. Cherfaoui, V. Marion, and J. G. Morillon. Leader-follower function for autonomous military convoys. In *Proceedings of SPIE Unmanned Ground Vehicle Technology VI*, volume 5422, pp. 326-337, 2004.

T. Vicsek, A. Czirok, E. Ben Jacob, I. Cohen, and O. Schochet. Novel type of phase transitions in a system of self-driven particles. In *Physical Review Letters*, volume 75, pp. 1226-1229, 1995.

A. Winfield. Distributed sensing and data collection via broken ad hoc wireless connected network of mobile robots. In *Proceedings of Fifth International Symopsium on Distributed Autonomous Robotic Systems, (DARS)*, 2000.

M. G. Wing, A. Eklund, and L. D. Kellogg. Consumer-grade Global Positioning System (GPS) accuracy and reliability. In *Journal of Forestry*, volume 105(4), pp. 169-173, 2005.

J. Wu, M. McDonald, M. Brackstone, Y. Li, and J. Guo. Vehicle to vehicle communication based convoy driving and potential applications of GPS. In *Proceedings of the 2nd International Workshop on Autonomous Decentralized System*, pp. 212-217, 2002.

E. Yoshida, T. Arai, J. Ota, and T. Miki. Effect of grouping in local communication system of multiple mobile robots. In *Proceedings of the IEEE/RSJ/GI International Conference on Intelligent Robots and Systems '94. 'Advanced Robotic Systems and the Real World', IROS '94.*, volume 2, pp. 808-815, 1994.